Rowan University

Rowan Digital Works

12-21-2020

Exploring a platinum nanocatalytic microcombustion-thermoelectric coupled device

Dylan Moore McNally
Rowan University

Recommended Citation
McNally, Dylan Moore, "Exploring a platinum nanocatalytic microcombustion-thermoelectric coupled device" (2020). *Theses and Dissertations*. 2853.
https://rdw.rowan.edu/etd/2853

EXPLORING A PLATINUM NANOCATALYTIC MICROCOMBUSTION-THERMOELECTRIC COUPLED DEVICE

by

Dylan M. McNally

A Thesis

Submitted to the
Department of Mechanical Engineering
Henry M. Rowan College of Engineering
In partial fulfillment of the requirement
For the degree of
Master of Science in Mechanical Engineering
at
Rowan University
November 23, 2020

Thesis Chair: Smitesh D. Bakrania, Ph.D.

Dedications

I would like to dedicate this manuscript to my mother, Donna, for her unrelenting support throughout my academic education. Her incredible ability to grasp, discuss, and even develop scientific theories has always astounded me and continues to amplify my own interest in science and engineering. I also dedicate this to my father, Richard, for his constant encouragement and assistance that enabled me to complete six years of undergraduate and graduate studies.

Acknowledgements

Abstract

Dylan M. McNally
EXPLORING A PLATINUM NANOCATALYTIC
MICROCOMBUSTION-THERMOELECTRIC COUPLED DEVICE
2011-2020
Smitesh D. Bakrania, Ph.D.
Master of Science in Mechanical Engineering

This work aimed to create a first-generation power device for eventual application to portable electronics. A platinum nanoparticle catalytic substrate was employed in a microcombustion-thermoelectric coupled (MTC) device for the purpose of chemical-to-electrical energy conversion. Multiple microcombustion reactors were designed, fabricated, and investigated. Most importantly, the reactor configuration was designed to accommodate thermoelectric generators (TEGs) for power production. Temperature studies with catalytic combustion of methanol-air fuel mixtures were used to evaluate the thermal power generation performance of each reactor. The final reactor design enabled ignition at room temperature with the ability to achieve repeat catalytic cycles upon subsequent exposure to methanol-air mixtures. Preliminary performance studies achieved a maximum temperature difference ΔT of 58 ^{o}C with a fuel mixture flow rate of 800 mL/min. While the temperature difference indicates a respectable potential for power generation, the importance of thermal design was a key finding of this work. It was thought that improved thermal management could make better use of thermal energy lost in the exhaust stream, potentially increasing reactor surface temperatures and corresponding thermoelectric generator parameter ΔT. Thermal design changes would significantly enhance the performance of a later generation of this device, detailed at the close of this thesis.

Table of Contents

List of Figures

List of Figures (Continued)

List of Tables

Chapter 1

Introduction

Portable power generation is in high demand due to a rising number of portable electronic gadgets. Personal, medical, and military applications alike require increasingly longer operational times and high energy densities. Such power devices must be compact, as well as efficient and durable. Currently, this demand is met with traditional batteries, which have low energy densities, are inefficient, and are hazardous to the environment. Recent research has investigated several potentially portable techniques of converting hydrocarbon fuels to electricity. Liquid hydrocarbon fuels have much higher energy densities than batteries, approximately 45 MJ/kg versus 0.5 MJ/kg for the most advanced alkaline lithium-ion devices [1, 2, 3]. Therefore, a system utilizing the combustion of liquid hydrocarbons would need to be just 1% efficient to match the performance of lithium-ion batteries. Direct methanol fuel cells (DMFCs) produce electricity from methanol. Unfortunately, the cells exhibit low voltages and the methanol fuel must be diluted, resulting in low energy density [3]. Proton exchange membrane (PEM) fuel cell systems take a different approach by generating power directly from hydrogen [2, 3]. An ideal PEM fuel cell has high energy density and efficiencies up to 70%. However, when the issues of fuel reforming and hydrogen storage are considered, energy density and efficiency is decreased and the system becomes very complex. Karim et al. predicted a PEM fuel cell system efficiency of 1.5% [4].

Microcombustors generate thermal energy from the combustion of hydrocarbon fuels. Once integrated with devices such as thermoelectric and thermophotovoltaic generators, the thermal energy is converted to electricity. These devices are simple when compared to complex fuel cell systems, and can be easily recharged with the addition of more fuel. Homogeneous combustion in

microcombustors produces a high-temperature flame, usually greater than 1500 ºC, which generates thermal energy [3]. Using a catalyst to combust the hydrocarbon fuel lowers operating temperature, and results in no flame. When considering these devices as a potential replacement for batteries, lower operating temperature is desired. However, combustion with lower operating temperature is more difficult to sustain due to heat loss. Thus thermal management becomes very important in such systems.

At Rowan University, Applegate et al. [5] demonstrated a platinum nanoparticle-coated cordierite substrate capable of room temperature ignition and repeatable, stable combustion of methanol in a flow reactor. Such a catalytic substrate is essential in a microcombustor-thermoelectric device so that operating temperature and power output may be accurately predicted and duplicated. This research sought to design, fabricate, test, and analyze a microcombustion-thermoelectric coupled (MTC) device that would utilize the previously mentioned nano-catalytic substrate. Much of the completed work was reactor-related due to the reactor's high influence on combustion and performance characteristics. The reactor was designed, and redesigned, based on comparative heat transfer simulations, combustion studies, and the specifications of available thermoelectric generator (TEG) modules. Generator studies were conducted with the final MTC device after optimization of the primary components.

The ultimate objective of this work was to create a first-generation power device that could eventually be used in portable applications. Incorporation of an existing, proven, catalytic substrate, that which was demonstrated by Applegate et al. [5], was a key element in this power device. The original reactor was replaced with one designed and optimized for integration with thermoelectric generator modules. The geometric mismatch between the catalytic substrate and the thermoelectric

generators was a key design criterion for this effort. The intention was to create a device that not only sustains microcombustion but also provides a source of power. The resulting microcombustion-thermoelectric coupled device and associated design efforts are described in this thesis.

1.1. Previous Work from Literature

A number of researchers have investigated the integration of microcombustion devices with thermoelectric generators (TEGs), several of which are discussed here. More details can be found in the summary table, Table 1. Vican et al. [6] designed a Swiss-roll concept reactor coupled with thermoelectric modules resulting in a chemical-to-electrical energy conversion efficiency of ~0.44% to 0.57%. The Swiss-roll reactor geometry enables the use of high-temperature exhaust gases to preheat the reactants, creating a self-sustaining combustion reaction. Vican et al. demonstrated sustained combustion both with and without a catalyst. A group of researchers at the University of Delaware, Federici et al. [3], conducted similar experiments with a catalytic microcombustor coupled to thermoelectric modules. This work was partially focused on thermal management of the heat transfer from reactor to thermoelectric generator. Thermal spreaders were used to create a uniform surface temperature at the TEG module interface, and a compressive load was applied to increase thermal contact. The same group had previously shown auto-ignition when using hydrogen fuel with a platinum catalyst. Federici at al. demonstrated a conversion efficiency of ~0.8%. Karim at al. [4] expanded upon this work two years later by increasing reactor size, achieving a conversion efficiency of 1.1%. Yoshida et al. [7] created a microcombustor capable of sustained combustion of butane or hydrogen. When coupled to thermoelectric modules, self-sustaining combustion was possible only with hydrogen, and resulted in a power output of 184 mW and a conversion efficiency of 2.8%. Marton et al. [8] obtained the greatest observed power output for a

microcombustor integrated with thermoelectric generators. Using a silicon reactor with butane fuel and a platinum catalyst, the group demonstrated a 5.82 W output for a conversion efficiency of 2.53%.

Table 1

Summary of prior research efforts investigating the integration of microcombustion devices with thermoelectric generators (TEGs).

Author	Article Title	Catalyst	Fuel	Reactor Design	Thermoelectric Coupling	Power & Efficiency
Vican et al. 2002 [6]	Development of a microreactor as a thermal source for microelectromechanical systems power generation	Platinum	Hydrogen	Swiss-roll, 2 channels with cross-section of 800 μm ^{2}, length of ~0.1 m	Two modules, Melcor Hot 2.0-31-F2A, and two cold reservoirs	Chem-to-elect: ~0.44% to 0.55%
Federici et al. 2006 [3]	Catalytic microcombustors with integrated thermoelectric elements for portable power production	Platinum, 8 nm particle size	Hydrogen, Propane	316SS plates and alumina insulation, 6 cm x 1 cm x 300 μm microchannel	One module, Hi-Z HZ-2, copper thermal spreader	Chem-to-elect: ~0.8%
Yoshida et al. 2006 [7]	High-energy density miniature thermoelectric generator using catalytic combustion	Platinum	Butane, Hydrogen	Silicon substrate bonded to glass, 2 combustion chambers 8 mm x 8 mm x 0.4 mm	Two modules, custom BiTe	184 mW, Chem-to-elect: 2.8%
Karim et al. 2008 [4]	Portable power production from methanol in an integrated thermoeletric/microreactor system	Platinum, ~4.5 nm particle size	Methanol	316SS plates and alumina insulation, 6 cm x 1 cm x 540 μm microchannel	One module, Hi-Z HZ-2, copper thermal spreader	0.65 W, Chem-to-elect: 1.1%
Marton et al. 2011 [8]	Portable thermoelectric power generator based on a microfabricated silicon combustor with low resistance to flow	Platinum, 3.6 μm particle size	Butane	Silicon reactor, 48 channels 1 mm x 1.05 mm x 35 mm	Two modules, Hi-Z HZ-2, graphite thermal spreader, forced air-cooled heat sinks	5.82 W, Chem-to-elect: 2.53%

1.2. Previous Work at Rowan University

Previous work at Rowan University by Applegate et al. [5] included the development of a reactor designed to support a platinum nanoparticle-coated substrate for combustion experiments. The reactor was a cylindrical tube, with an NPT fitting at the inlet for coupling to a gas line, and an open outlet where the substrate could be inserted. The reactor is shown in Fig. 1. A flange was created at the outlet of the reactor for coupling to a gas chromatograph for conversion studies. Grooves were cut into the surface to maximize convection cooling with increased surface area. Although the work in this thesis would prove that increased heat loss is a negative characteristic, the low thermal mass of Applegate's reactor enabled sustained combustion [5].

(a)　　　　　　　　　　　　　(b)
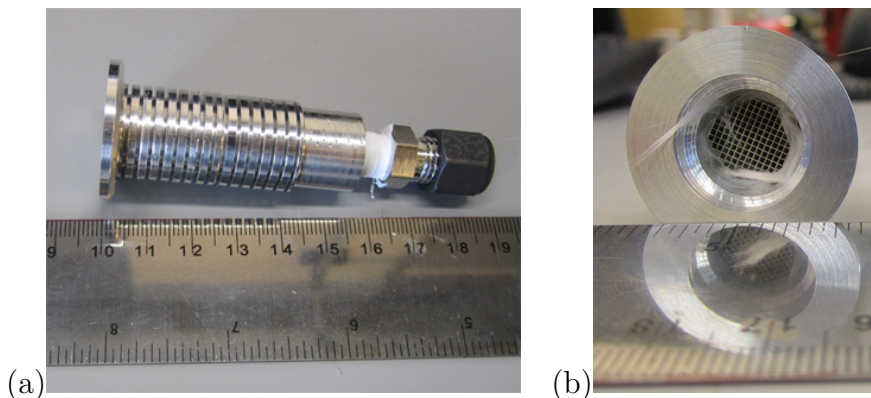
Figure 1. The reactor used by Applegate et al. [5] at Rowan is shown (a) from the side and (b) from the outlet. A substrate surrounded by quartz wool insulation can be seen inside the reactor.

Blank substrates were cut from a cordierite monolith, shown in Fig. 2, and coated with a Pt nanoparticle solution. Coated substrates were wrapped in quartz wool to prevent flow of gas around, rather than through, the coated channels. A 0.5-mm, K-type thermocouple was cemented inside the substrate during experiments to study combustion temperatures.
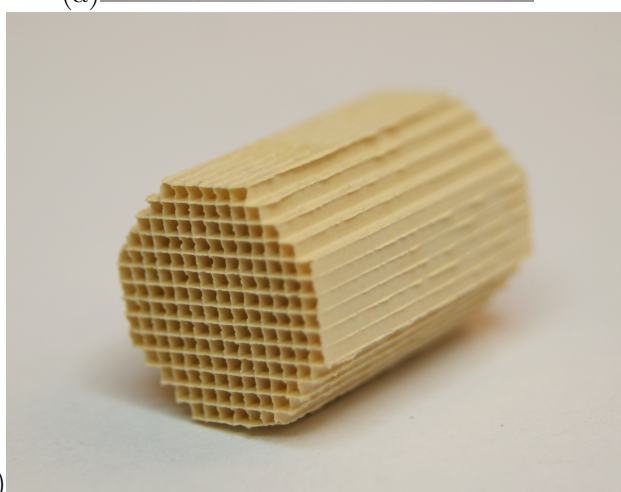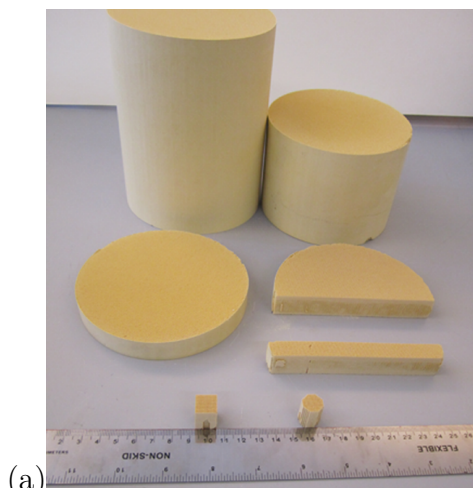
Figure 2. The cordierite substrate (a) as it is cut to size from the original monolith and (b) a close up of the final blank substrate used in testing.

Tests were conducted by flowing a methanol-air mixture through the reactor for 30 mins, and then shutting the flow off and allowing the reactor to cool for 30 mins. This 30 mins on, 30 mins off cycle was continued several times to study the repeatability of combustion temperatures and catalytic activity. Results demonstrated that the nanocatalytic substrate was able to combust the methanol-air mixture at room temperature, so that neither preheating the reactants, nor the use of hydrogen, often present in other studies, was necessary. Combustion was extremely stable, and could be repeated for over 20 cycles without significant change in combustion temperatures. A run of three cycles is shown in Fig. 3. This particular

test was conducted with a mixture flow rate of 600 mL/min and a substrate coated on all four sides. Although ex-situ sintering studies conducted through a separate test method demonstrated degradation of the catalysts at high temperature, repeatable cycling shows that particle sintering has a minimal effect on catalyst performance. In addition to the cycling studies, an extended combustion run was conducted for approximately 6 hours. After 3 hours of continuous operation, temperature began to waver, indicating a change in catalyst stability.
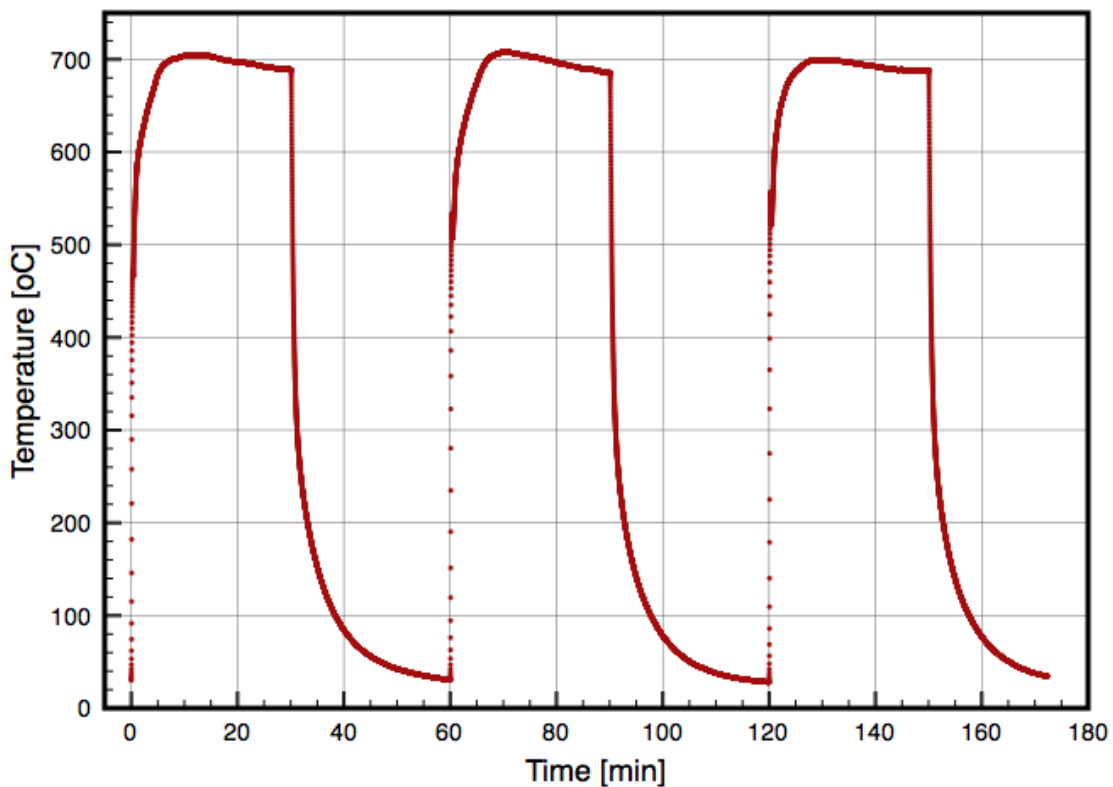
Figure 3. Temperature profile of a 3-cycle run demonstrating room temperature ignition and highly repeatable catalytic cycling. The substrate was coated on all four sides and the flow rate was maintained at 600 mL/min.

Studies involving various flow rates demonstrated that combustion temperatures generally increase as flow rate increases. Figure 4 depicts the temperature profiles for nine runs, each with a different flow rate ranging from

200-1000 mL/min, in 100 mL/min increments. As flow rate approaches 1000 mL/min, temperatures increase by smaller increments until they no longer increase at all. This can be explained by the decrease in residence time of the fuel as flow rate increases. Each run was conducted with a substrate coated on all four sides.
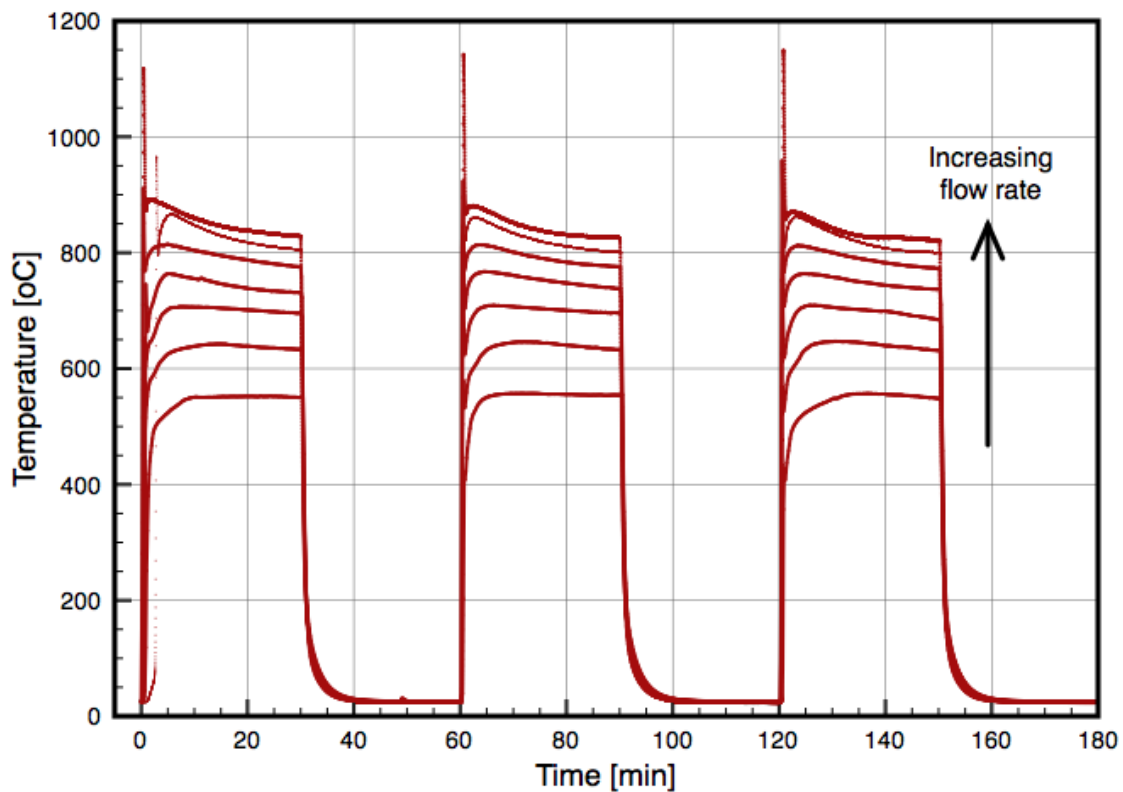
Figure 4. Temperature histories for air flow rates ranging 200-1000 mL/min with 100 mL/min increments. Catalyst substrates with four Pt-coated sides were used in this study.

Mass loading studies were conducted by running substrates with varying number of coated sides. Figure 5 shows that combustion temperatures increase slightly, as the number of coated sides increases. The change in temperature is minimal for each additional coating, but there remains a clear trend. All tests used a flow rate of 200 mL/min.
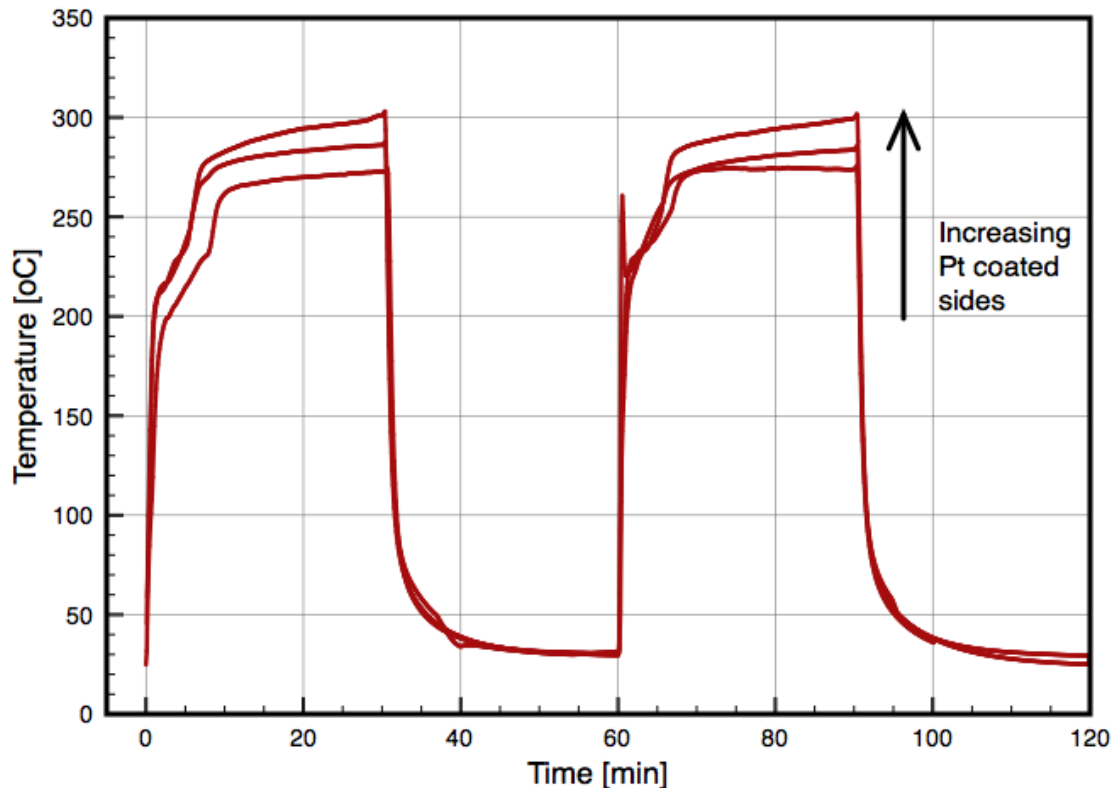
Figure 5. Temperature histories for substrates with two, three and four Pt coated sides with air flow rate at 200 mL/min.

Gas chromatography was performed to study the quantity of methanol that was combusting for each type of experiments. Results indicated that the greatest conversion percentage, approximately 60%, was occurring with lower flow rates, and higher mass loadings.

This work indicated the potential of a catalytic substrate capable of auto-ignition of a methanol-air fuel mixture. However, the combustion reactor lacked the necessary configuration to couple with planar thermoelectric modules for the purpose of portable power generation. The need for a redesigned, thermally optimized combustion reactor with geometry appropriate for use with thermoelectric modules was warranted. The challenge was to develop a reactor that not only provided better coupling with thermoelectrics, but provided ideal environment for

the catalytic action and sustained heat generation using the same catalytic substrate identified earlier.

Chapter 2

Background

2.1. Microcombustor

A microcombustor is defined as a reaction chamber having channel critical dimension of 1 mm or smaller [9]. At this dimensional scale, the surface area-to-volume ratio is significant, increasing heat loss. Higher heat losses make self-sustaining combustion more difficult to achieve, and quenching mechanisms dominate. Catalysts are used to lower combustion temperatures so that the problem of heat loss is reduced. Even with the use of a catalyst, however, thermal management remains very important for stable, self-sustaining combustion. Efficiency of a microcombustor may be characterized by assessment of fuel conversion rates. Fuel conversion rate is dependent on flow rate and reactor length (related to residence time), as well as fuel-air mixture and combustion temperature (related to combustion time). In order for complete combustion to occur, residence time must be equal to or greater than combustion time [1].

2.2. Catalysis

As mentioned above, catalysis is of great benefit to micro-scale combustion. Homogeneous combustion at the micro-scale is limited due to the nonpropagation of a high-temperature flame [9]. Therefore, combustion is highly localized and is heavily impacted by heat loss to the reactor mass. Presence of a catalyst extends the combustion region and lowers reaction temperature, increasing the odds of self-sustaining combustion. Although a catalyst improves combustion conditions, thermal management continues to be important in order to prevent reaction quenching.

Catalyst performance is greatly increased with smaller particle sizes, due to higher surface area-to-volume ratio. However, smaller particles will sinter at lower

temperatures, ultimately reducing surface area-to-volume ratio and performance. Previous work by Applegate et al. [5], discussed earlier, investigated the use of nano-sized platinum particles. This work involved assessment of the catalyst particles before and after various run times. It was found that cycling combustion lengthened the life of the catalyst, as opposed to continuous combustion. Also important is the portion of the fuel mixture exposed to the catalyst. Applegate et al. found that deposition of the catalyst on all substrate walls, thereby maximizing catalyst loading on the substrate, resulted in higher combustion temperatures.

2.3. Thermoelectric Generator

Many of the researchers investigating microcombustion for the purpose of power generation have used thermoelectric generators (TEGs) for direct conversion of thermal-to-electrical power [3, 6, 7, 8]. These generators are popular due to their mechanical robustness and desirable size [10, 11]. Thermoelectric modules have no moving parts and thus are highly durable as long as they are not subjected to temperatures above the rated material limit.

Thermoelectric power generation is governed by the Seebeck Effect, or the development of an electrical voltage when a material experiences a temperature gradient [10]. This relationship is given by the equation

$$S = V/\Delta T$$

where S is Seebeck coefficient, or thermopower, V is electrical voltage, and ΔT is the temperature difference. Thermoelectric generators are generally rated by the dimensionless Figure of Merit, given by the equation

$$ZT = S^2 \sigma T/k$$

where ZT is a material's Figure of Merit, S is Seebeck coefficient, σ is electrical

conductivity, and k is thermal conductivity [11]. Thermoelectric generator power output is calculated from key parameters such as Seebeck coefficient, module internal resistance (R_i), load resistance (R_L) and temperature differential. Maximum power is generated when $R_L = R_i$, leading to the the power equation

$$P_m = \Delta T^2 S^2 / 4R$$

where P_m is maximum power output and R is resistance. Device thermal efficiency is defined as generator power output divided by heat input to the thermoelectric hot side.

The key parameters mentioned above are known for commercial TEG modules, which enables prediction of power output based on theoretical hot- and cold-side temperatures. In the research discussed in this document, power output was not directly measured. Instead, theoretical power output was calculated from measured surface temperatures of the TEG modules. Module internal resistance was assumed to be equal to load resistance (known as load matching) for the prediction of maximum output.

Chapter 3

Objective, Hypothesis and Thesis Outline

With previous work showing possible room temperature combustion of methanol-air mixtures using platinum nanoparticles embedded in a cordierite substrate, the objectives of this work were to:

1. Develop a power device capable of electrical power generation with potential for use in portable applications.
2. Optimize power generation potential through the evolution of combustion reactor design.

These objectives were intended to expand upon previous research in catalytic microcombustion completed at Rowan University and apply prior achievements towards the creation of a microcombustion power generator. The platinum nanoparticle catalyst developed and tested at Rowan had demonstrated great potential for use in a power generator incorporating similar catalyst-substrate geometry and fuel mixtures. The researchers involved in this work decided the next steps were to design and fabricate new reactors, conduct combustion studies, and ultimately integrate the microcombustor with thermoelectric generators.

It was hypothesized that a cordierite-based nano-catalytic substrate would be ideal for use in a specially designed microcombustion-thermoelectric coupled (MTC) device. Previous work had already demonstrated repeatable, self-sustaining combustion of a methanol-air fuel mixture using a platinum nanoparticle catalyst deposited in a cordierite substrate. Auto-ignition of the fuel mixture was achieved and combustion temperatures were considered sufficient for thermoelectric power generation. Design of a new reactor and subsequent combustion and temperature studies were necessary to integrate with and maximize efficiency of a thermoelectric module.

Chapter 1 of this thesis provides an introduction to the field of microcombustion power generation. Prior research at Rowan University and conducted by other researchers is reviewed. Chapter 2 covers background information for three primary components involved in this work, the microcombustor, catalyst, and thermoelectric generator. Chapter 3 states the overall objective for this work and the researchers' hypothesis. Chapter 4 describes all experimental procedures involved with this effort. This includes catalyst synthesis and preparation, test procedures, and device materials and assembly. Chapter 5 is a discussion of the researchers' findings. Results are given for combustion studies, the reactor design and modeling effort, and final integration with thermoelectric generators. Chapter 6 provides concluding comments and discussion. Chapter 7 reviews follow-on studies conducted at Rowan University in the time since completion of the work discussed in this thesis.

Chapter 4

Experimental

4.1. Pt Nanoparticle Synthesis

A wet chemical method reported by Bonet et al. [12] was used to synthesize platinum nanoparticles. To begin, 45 mL of ethylene glycol (EG, 99.8%, Sigma Aldrich) was added to a reflux reactor and placed in an oil bath. The oil bath was heated up to 150 ^{o}C using a hot plate. While heating, two solutions were made. Solution 1 was made by dissolving 500 mg of hexachloroplatinic acid (H_2PtCl_6, ACS reagent grade, Sigma Aldrich) in 5 mL of EG. Solution 2 was made by dissolving 100 mg of polyvinylpyrrolidone (PVP, M.W. 29,000, Sigma Aldrich) in 25 mL of EG. Before adding solutions, a magnetic stirrer was added to the reflux reactor. Once the oil bath was at 150 ^{o}C, Solution 1 was added to the reflux reactor. Solution 2 was added to the reactor at a rate of 1.5 mL/min using a peristaltic pump. When both solutions were combined with the EG in the reflux reactor, the final solution was held at 150 ^{o}C for one hour. After one hour, the reactor flask was removed and held under cold, running water to rapidly cool the nanoparticle solution. The cool solution was placed in a capped container for storage. After several hours, particles fell out of solution so it was always necessary to agitate the container before use.

Before using the Pt nanoparticles, the solution had to be cleaned in order to remove the EG and PVP. To do this, 5 mL of EG-PVP-Pt nanoparticle solution was mixed with 25 mL of methanol (99.8%, Sigma Aldrich) in a centrifuge tube. The centrifuge tube was agitated by hand before centrifuging for 2 min, at 3,000 rpm. The supernate was drained and 25 mL of deionized water was added. If particles were stuck to the sides of the tube, a plastic stir was used to manually scrape them off. The centrifuge tube was again agitated by hand and then by a vortex mixer. These agitation steps were repeated until all particles were again suspended in the solution.

Then the tube was centrifuged for 2 min at 3,000 rpm. The supernate was drained and 5 mL of deionized water was added. Agitation and manual scraping steps were performed until the particles were fully suspended. The solution was poured into a small beaker and sonicated at full power for one minute. Once cleaned, particles were used within 2 days. After 2 days, leftover cleaned particles were discarded. Before deposition, the solution was always agitated to stir up particles that had settled.

4.2. Substrate Preparation

Substrates were cut from a cordierite monolith (Corning Inc.). The base monolith was a cylinder with a length of 154 mm and diameter of 114 mm. A cross-section of the monolith had a cell density of 139.5 cells per square cm (900 cells per square inch), each cell with a width of 0.85 mm and wall thickness of 0.05 mm. A bandsaw was used to cut disks of 19.05 mm (0.75 in) in length. The disks were cut into 14 x 14 cell squares using a razor blade. This was done by counting out 14 rows of cells in one direction and scoring the 15th row of cells along the entire disk. A tool was used to tap the razor blade into the resulting groove to break the disk along the 15th row of cells. This process left a long section of disk 14 cells wide. The ends of this strip were cut to remove the curved portions. A 14 x 14 cell square was created by counting 14 cells in from one end of the long strip, and cutting on the 15th. To round the substrate, the 4 corners were cut at 45° angles so that 6 cells were left intact along each of the 4 straight sides, as shown earlier in Fig. 2. Blank substrates were cleaned with methanol and acetone, respectively, and then dried using compressed air. This step was performed just before the first deposition on each substrate.

4.3. Nanoparticle Deposition

A draw coat method was used to deposit Pt nanoparticles on a substrate. The end of a syringe with a diameter of 15 mm was removed so that a substrate could fit inside comfortably. Modeling clay was used to create a seal between the substrate

and syringe. A 3 mL dish was filled with cleaned Pt nanoparticle solution. The substrate was lowered into the dish, and the syringe plunger was drawn upward to draw solution into the cells. The clay seal was broken so that excess solution ran back into the dish. This procedure is depicted in Fig. 6.
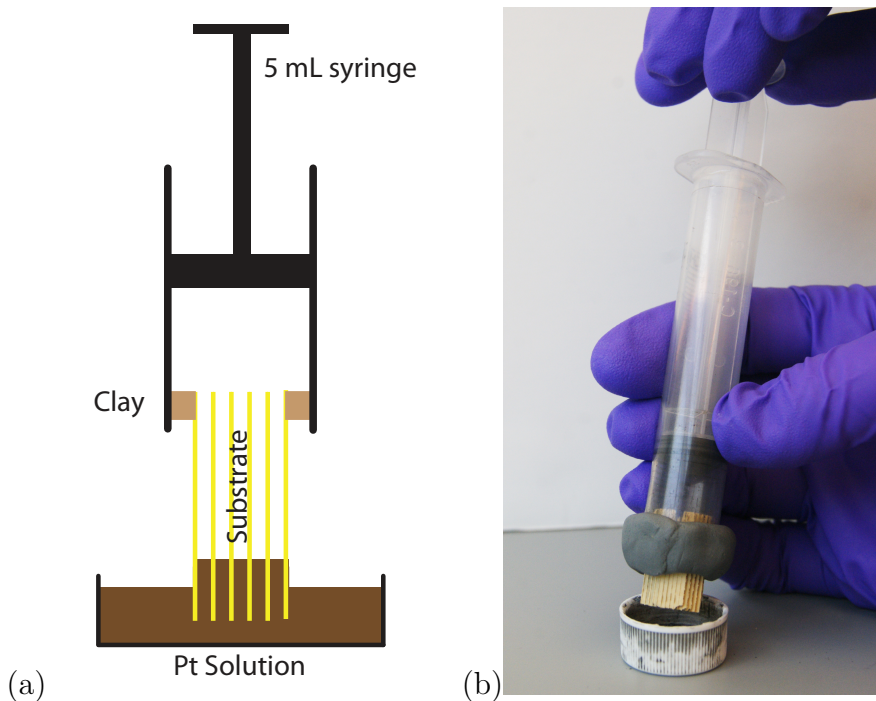
Figure 6. Setup for coating the cordierite substrate. Using a 5 mL syringe attached to the substrate using a flexible clay gasket, 2 mL of Pt solution is drawn into the substrate. Subfigure (a) provides a schematic of the process and (b) shows the physical setup.

The substrate was then placed horizontally on its side in a petri dish inside a fume hood to dry. The drying time varied due to humidity and air flow levels inside the building. If necessary, a computer fan and dry box were used to speed up the process. Substrates were considered dry when all channels are visibly clear and unblocked. During the drying process, the bulk of the deposited platinum rested on the bottom side of the substrate channels. By rotating the substrate after subsequent coatings, multiple sides were coated. Typically, this was done by coating one side

19

at a time and then rotating 180°, 90°, and 180°, with respect to the previous coat, as seen in Fig. 7. Marks were placed on the substrate to distinguish the four sides. Approximately 2 mL of solution was deposited inside the substrate with each coat. The solution was calculated to contain 5 mg of Pt nanoparticles per mL of solution, or 10 mg per coat. All experiments were conducted with one of two coating patterns, two opposite sides single-coated (2SSC) and four sides single-coated (4SSC).
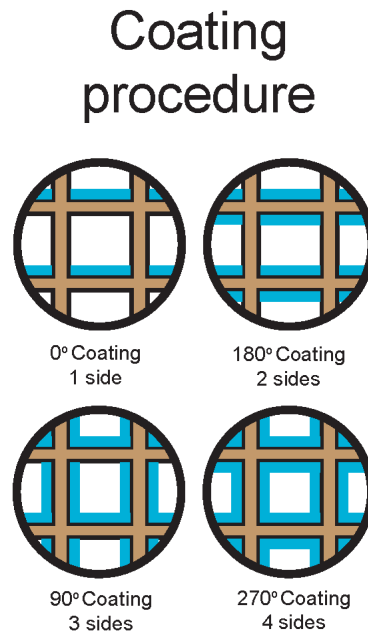
Figure 7. The process for coating multiple substrate walls is shown. Each deposition coats a single wall.

4.4. Microcombustion-Thermoelectric Coupled Device Assembly

The microcombustion-thermoelectric coupled (MTC) device assembly consisted of a reactor, which housed the substrate, sandwiched between two thermoelectric modules and two heat sinks. Many early experiments were conducted with varying assemblies, and all components used are discussed in this section. One of two base reactor designs was used for each experiment. The dimensions of each reactor depended on substrate and thermoelectric generator dimensions. Reactors

were drawn in SolidWorks before fabrication. Reactor 1 consisted of a 63.5 mm x 63.5 mm x 25.4 mm (2.5 in x 2.5 in x 1 in) block of 6061 aluminum alloy. A dimensioned drawing and an image of Reactor 1 is shown in Fig. 8. The outlet channel diameter was designed larger than the inlet channel so that a substrate could easily be inserted until it contacts the smaller inlet channel. The inlet was threaded with a 1/4-18 NPT tap and the outlet was threaded with a 3/8-18 NPT tap to allow for coupling to the test facility.
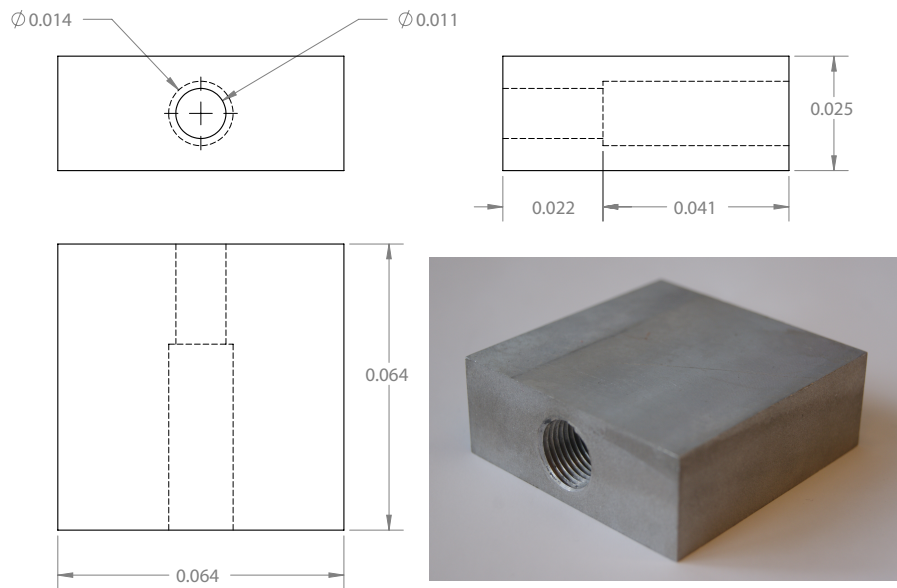
Figure 8. A dimensioned drawing and image is shown of Reactor 1. Units are in meters.

Reactor 2 was designed to account for several design flaws in Reactor 1. It consisted of a 30.48 mm x 30.48 mm x 20.32 mm (1.2 in x 1.2 in x 0.8 in) block of 6061 aluminum alloy with 2.54 mm x 20.32 mm (0.1 in x 0.8 in) flanges on the inlet and outlet sides. A dimensioned drawing and an image of Reactor 2 is shown in Fig. 9. The outlet channel diameter was designed larger than the inlet channel so that a substrate could easily be inserted until it contacts the smaller inlet channel. The inlet

was threaded with a 1/4-18 NPT tap and the outlet was threaded with a 3/8-18 NPT tap to allow for coupling to the test facility. A 9/16-in ball mill was used to remove material on the sides parallel to the channel to decrease thermal mass. Grooves were cut on the top and bottom of the reactor using a 1/32-in end mill for placement of surface thermocouples. Creating grooves to house the thermocouples ensured that the thermoelectric generators would be flush with the reactor surface.
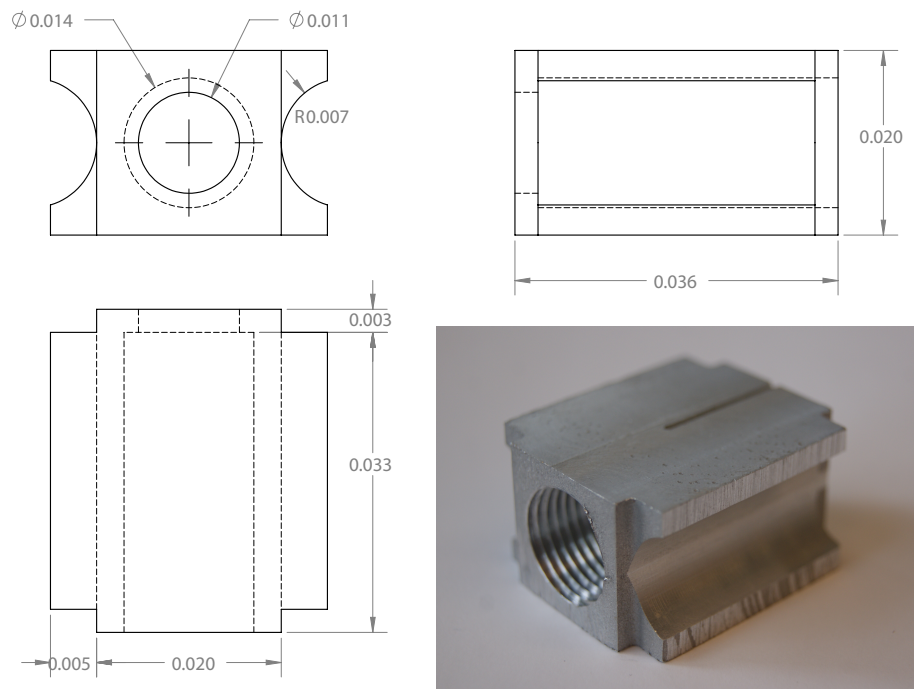
Figure 9. A dimensioned drawing and image is shown of Reactor 2. Units are in meters.

Several types of heat sinks were used to determine which size was best to use with Reactor 2. All small and medium size sinks were pulled from old computers. The large heat sinks were purchased from Hi-Z Technology, Inc. From left to right, two small sinks, two medium sinks, and one large sink are shown in Fig. 10. Sizes range from 31 mm x 34.5 mm x 34.5 mm (1.22 in x 1.36 in x1.36 in) to 152.4 mm x

152.4 mm x 63.5 (6 in x 6 in x 2.5 in). Grooves were cut on the bottom of all heat sinks using a 1/32 in end mill for placement of thermocouples.
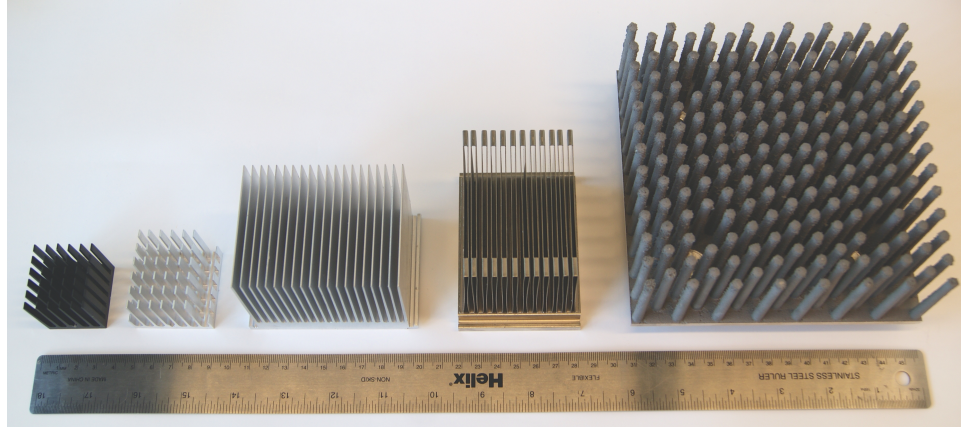
Figure 10. All heat sinks used during testing are shown. The heat sink second from the right was used in the final assembly.

Two types of thermoelectric generator (TEG) were used. The HZ-14 thermoelectric module (Hi-Z Technology, Inc.) has dimensions 62.7 mm x 62.7 mm x 5.08 mm (2.47 in x 2.47 in x 0.2 in), can generate a maximum output of 13 W, and was used with Reactor 1. The HZ-2 thermoelectric module (Hi-Z Technology, Inc.) has dimensions 29 mm x 29 mm x 4.32 mm (1.15 in x 1.15 in x 0.17 in), can generate a maximum output of 2.5 W and was used with Reactor 2. Both modules generate maximum output when the hot side temperature is 230 ^{o}C, and the cold side temperature is 30 ^{o}C. While temperatures above 230 ^{o}C were never observed, this was considered the maximum temperature the modules could withstand. These modules can be seen in Fig. 11. Thermal grease (Hi-Z Technology, Inc.) was applied on thermoelectric generator and heat sink surfaces to ensure good contact.
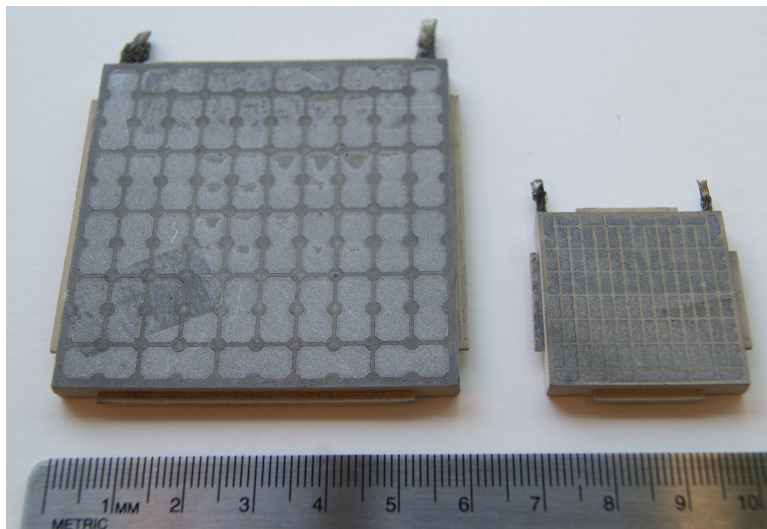
Figure 11. The HZ-14 (left) and HZ-2 (right) thermoelectric modules are shown. The hot side of each is distinguishable by the circular nodes.

A ceramic insulation (Rescor 902 Machinable Alumina Silicate, Cotronics Corp.) having a thermal conductivity of 1.298 W/mK was used with Reactor 1 in an attempt to limit heat loss. A block of ceramic with dimensions 152.4 mm x 152.4 mm x 25.4 mm (6 in x 6 in x 1 in) was cut and bored to accommodate Reactor 1, as seen in Fig. 12.
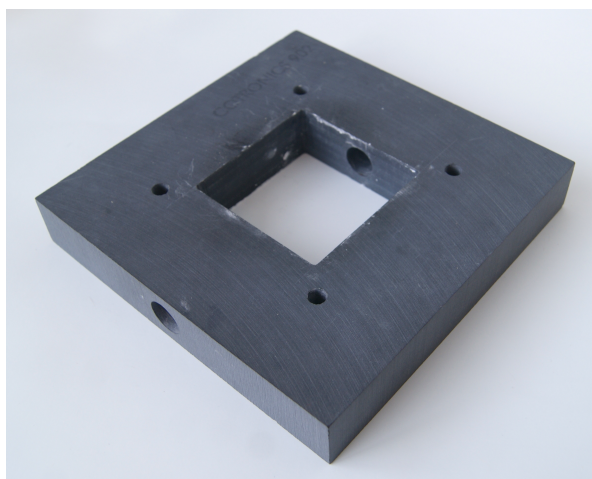
Figure 12. Machined ceramic insulation for use with Reactor 1 is shown.

4.5. Testing Methodology

Experiments were conducted by flowing a methanol-air mixture through a substrate coated in Pt nanoparticle catalyst and measuring combustion temperatures. The methanol-air mixture was created by using a mass flow controller (4 channel, MKS) to flow compressed air (99.9%, Airgas) through a glass bubbler inserted into a 250 mL flask containing methanol (99.8%, Sigma-Aldrich). The reactor was positioned after the bubbler to provide a combustion chamber for the catalytic substrate. A solenoid valve between the air tank and the flow controller was activated by a timer program to turn air flow on and off. This program was adjusted to each run so that flow would cycle on and off autonomously. Air flow rates of 400-800 mL/min were programmed into the flow controller via the instrument user interface. The air tank regulator was set to a pressure of less than 68.95 kPa (10 psi) to prevent harming the mass flow controller and to maintain a safe pressure in the methanol flask. Thermocouples (K-Type, Omega) were placed inside the substrate and on reactor and heat sink surfaces, when desired. These were connected to a thermocouple input module (16-channel, National Instruments), which was in turn connected to the computer. A Labview program was used to record temperature data over time and write it to a text file. A schematic of the final bubbler and MTC assembly is shown in Fig. 13.
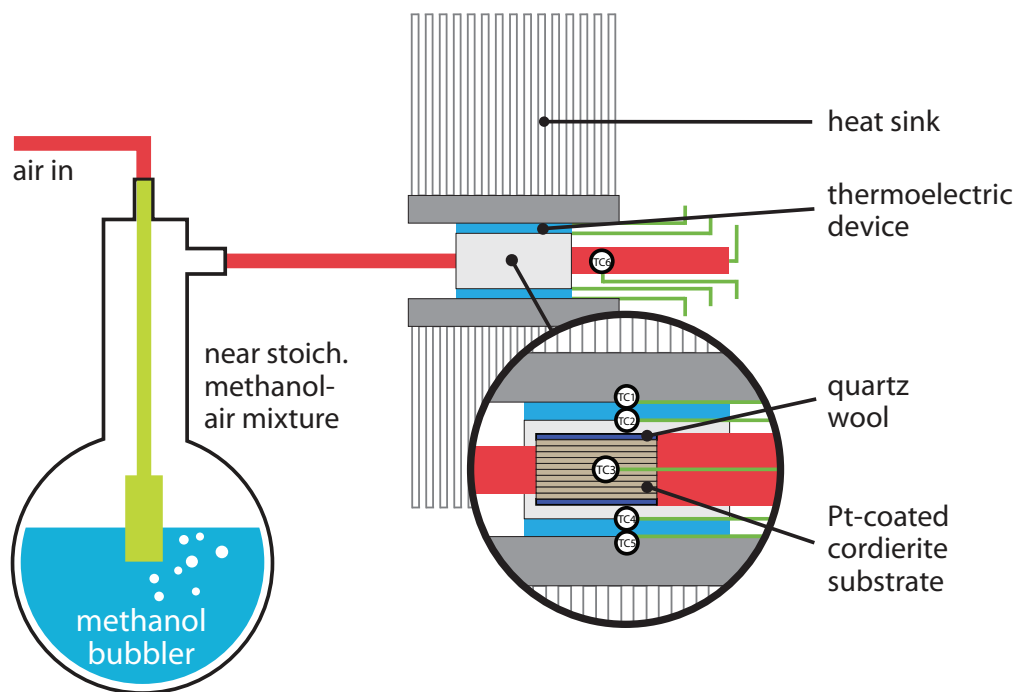
Figure 13. Air enters the bubbler after passing through the mass flow controller (not shown) and the resulting methanol-air mixture enters the reactor where it combusts. Power device assembly with thermoelectric generators and heat sinks are shown. Inset depicts a catalytic substrate inside the reactor, and locations of all thermocouples. Note: Assembly has been rotated 90º so that all components are visible. Not drawn to scale.

To begin an experiment, a dry, coated substrate was prepared. Quartz wool was used to insulate the substrate and prevent the fuel-air mixture from flowing around the substrate, rather than through it. The quartz wool was cut into 19.05 mm x 152.4 mm (0.75 in x 6 in) strips or a mass of approximately 0.1 g, and wrapped tightly around the substrate. It was found that cutting these strips parallel to the axis of the roll of quartz wool was the best method to keep the strip from pulling apart while wrapping. A coated substrate wrapped in quartz wool is shown in Fig. 14. Once wrapped, a thermocouple was inserted 7.62 mm (0.3 in) deep into one of the center channels of the substrate. A metal clip was placed on the thermocouple wire so that it would be inserted the correct depth, and high temperature cement

(#CC High Temp, Omega) was used to secure it. The cement was allowed to dry for at least 30 min before testing.

Figure 14. A coated substrate (2SSC) is wrapped in quartz wool in preparation for testing.

In order to limit sustained exposure of the nanoparticles to high temperatures, fuel flow was cycled on and off. Cycles of one hour (30 mins on and 30 mins off) allowed combustion temperatures inside the substrate to stabilize while the fuel supply was on, and allowed the substrate to cool to room temperature while the fuel supply was shut off. Up to three consecutive cycles were run for each experiment.

Chapter 5

Results and Discussion

This chapter discusses the combustion experiments and reactor development involved in this work. Section 5.1 provides the results of a series of combustion experiments conducted to determine the cause of the initial temperature spike present in most combustion cycles. While not directly related to the work discussed in the subsequent sections, it is mentioned first to introduce an interesting artifact in the results. Section 5.2 steps through development and testing of each reactor design, in chronological order. In other words, how the design evolved and the rationale behind each iteration. This chapter culminates in a discussion of the final microcombustion-thermoelectric coupled (MTC) device, in Section 5.3.

5.1. Temperature Spike

In both the previous and current work, a temperature spike, that was higher than the stable combustion temperature, was observed at the start of each cycle for all flow rates and mass loadings. It was surmised that the spike was due to a build-up of air in the gas lines, and therefore facility-related. Upon investigation of the mass flow controller, it was realized that the initial flow rate, when the controller first turned on, was much higher than the programmed value. After a few seconds, the flow rate would settle to the value programmed into the controller. To test this gas build-up theory, two valves were added to the air line, just before the bubbler. One was used to close off flow to the bubbler while the other was used redirect flow into the ambient environment. At the start of a test, the valves were adjusted to direct the air flow out of the system. The test was started, and the user studied the mass flow controller flow rate display. Once the flow rate settled to the desired value, the valves were readjusted to direct flow into the bubbler.

The results of the flow bypass test are shown in Fig. 15. The high-temperature

spike has been largely eliminated (refer to Fig. 4 in Section 1.2 for comparison to a series of tests demonstrating the temperature spike). A spike appears to exist due to the large dip in temperature at the beginning of each cycle. In reality, this is not a high-temperature spike, but a drop in temperature due the large thermal mass of Reactor 1, which causes extensive heat loss at the start of each cycle. More combustion characteristics of Reactor 1 are discussed in Section 5.2.1.b. The results of this test demonstrate that the increased flow at the start of each test, which comes as a result of gas build-up, has a direct impact upon the high-temperature spike. This confirms suspicions that the temperature spikes are facility-related, and can be largely eliminated by using a flow bypass system.
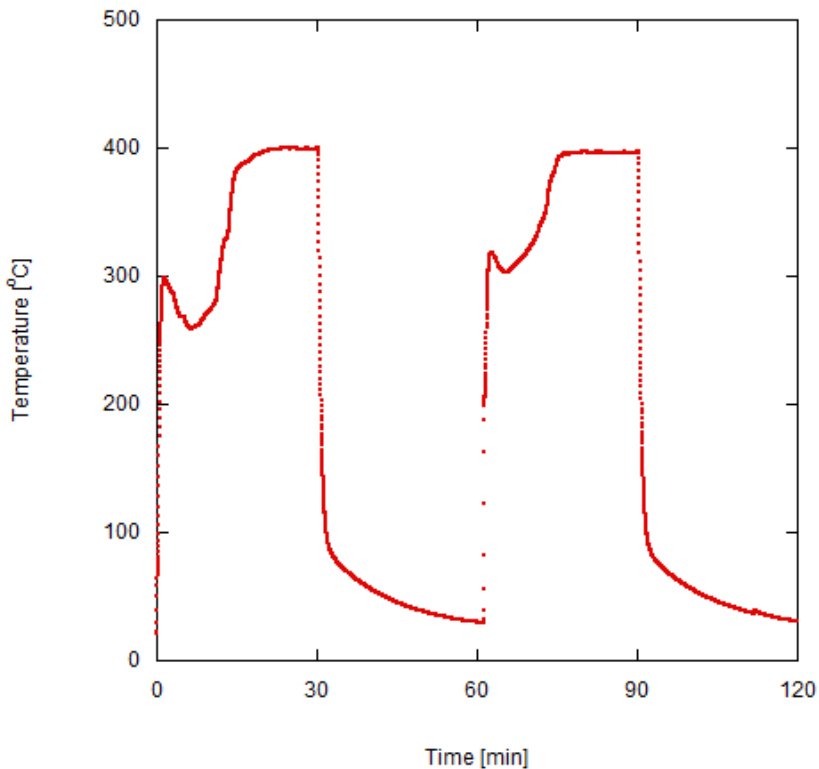
Figure 15. Substrate temperature for 1 run at 400 mL/min with 2 cycles when using bypass valves for a 4SSC substrate. High-temperature spike at the beginning of each cycle is largely eliminated. Temperature dip at the start is due to heat loss to the cool reactor.

Due to the inconvenience of using manually operated valves, and the major human error added when using the bypass system, all subsequent tests were done normally. Although the spike remains visible in most test results, a partial understanding exists for why it occurs.

5.2. Reactor Development

5.2.1. 2.5-inch planar design. This section discusses Reactor 1, the 2.5-inch planar design. The section is broken into two subsections, Development and Modeling, and Reactor Performance.

5.2.1.a. *Development and modeling.* In the design of a microcombustor-thermoelectric device, thermal management is extremely important. The reactor must retain enough thermal energy to sustain combustion, while still conducting a great deal of energy to the surfaces where the TEG's are placed. Uniform temperatures are desired on the reactor surface so that all areas of the thermoelectric generator are exposed to similar temperatures, and maximum efficiency is achieved. One method of achieving uniform temperatures while reducing heat loss is heat recirculation. This involves using the high-temperature exhaust gases to heat the reactor evenly, or to preheat the reactants. Because previous results with the Pt-nanoparticle catalytic substrate have demonstrated room temperature ignition, preheating the reactants was not a concern. The primary goal of heat recirculation, in this case, was to heat the reactor surfaces uniformly, and to reduce losses from the system. A second method of generating a uniform temperature distribution on the surface is to use thermal spreaders on the reactor surface. Thermal spreaders are made of highly conductive materials that will distribute thermal energy more evenly than the reactor material. If the reactor itself was fabricated from such a highly conductive material, massive losses in thermal energy would quench combustion. A thin thermal spreader placed between the reactor and thermoelectric generator

would create a uniform temperature distribution much more efficiently. Each of these design methods was considered during heat transfer simulations.

SolidWorks Flow Simulation was used to create solid models and analyze heat transfer in the reactor. The combustion reaction was not modeled, and a cylindrical volume at constant temperature was used as the heat source for the simulation. These simulations were steady-state, 3D, comparative models, and complete accuracy was not the ultimate concern. Each model was defined using similar initial and boundary conditions. All conditions were based on previous experimental results. Because heat recirculation is directly dependent on gas flow in the reactor, models utilized both the Navier-Stokes equations and the heat equation. Reactor dimensions were identical for each model (see Section 4.4 for dimensions). As stated earlier, reactor dimensions were chosen to match those of the thermoelectric generator model (HZ-14) and insulation block. The reactor subdomain was set as solid aluminum, a predefined material in SolidWorks. The surrounding insulation was set as alumina silicate with material properties from the Cotronics Corp. website. All solid and fluid subdomains were initially at room temperature, or 20 ^{o}C . A solid cylindrical heat source was used to mimic combustion in a catalytic substrate. The volume source temperature was set at 280 ^{o}C to account for the quartz wool insulation and lower combustion temperatures towards the back of the substrate. In order to define a flow rate of 400 mL/min, an inlet flow boundary condition was created on the outlet face of the substrate. The channel outlet pressure was defined to be environmental pressure at 101.3 kPa. Brass and copper thermal spreaders of 1.588 mm (0.0625 in) in thickness were added to the models for comparison. In each case, the aluminum reactor thickness was decreased to accommodate two thermal spreaders on the top and bottom faces. Each of these solid domains used predefined material properties in SolidWorks.

Three separate models were compared. Reactor 1a was the most simplistic

design, with a single, straight channel through the reactor, with the substrate in the center. Reactor 1b featured a substrate placed in one corner, with a single channel winding through the reactor with three 180° turns. Reactor 1c was much more complex with two separate channels originating from a centrally placed substrate, winding around the reactor, and recombining at a single outlet. Simulations were compared by studying surface temperature profiles on the reactor faces that would be flush with the thermoelectric modules. The model results predicted that Reactor 1a, the most simplistic design, would generate the most uniform surface temperature distribution. Reactor 1b demonstrated a highly skewed temperature distribution, due to the corner location of the substrate. In Reactor 1c, it was apparent that heat recirculation was creating the opposite of the desired effect, and removing heat from the reactor. Each model and the relative temperature distribution is shown in Fig. 16. Thermal spreaders did not seem to improve the uniformity of surface temperatures as much as previously thought, and results are not shown. After all simulations were complete, Reactor 1a was chosen as the most promising design, and fabricated. Figure 17 shows the initial device assembly in two sections. The following section describes design changes to the heat sinks and insulation that was used.
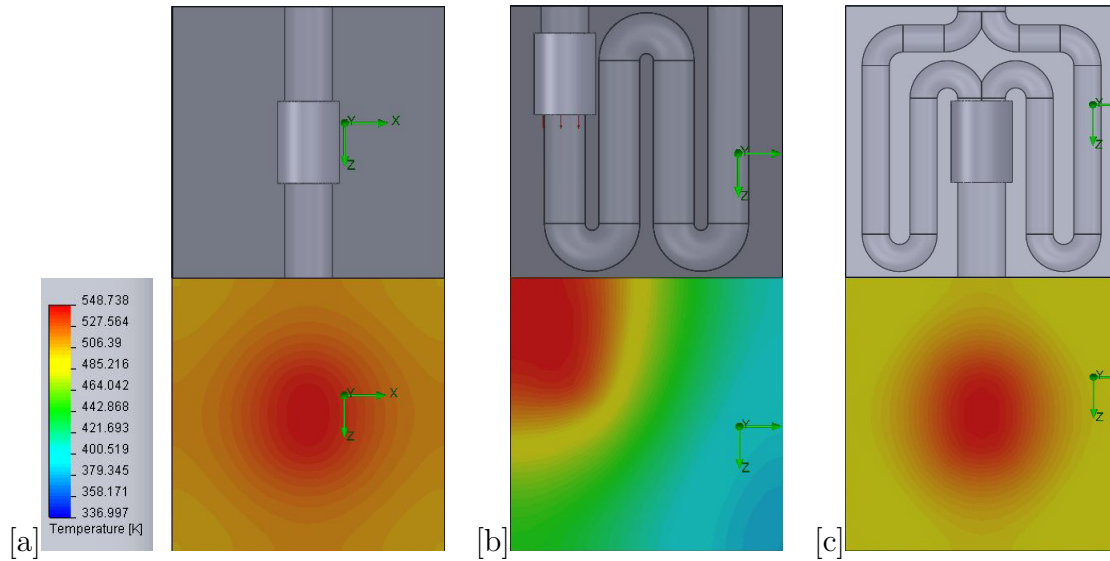
Figure 16. Each reactor design and the respective surface temperature distribution is shown. (a) Reactor 1a generates the most uniform temperatures. (b) Temperatures are highly skewed in Reactor 1b due to the corner location of the substrate. (c) In Reactor 1c heat recirculation removes thermal energy from the reactor rather than distributing it.
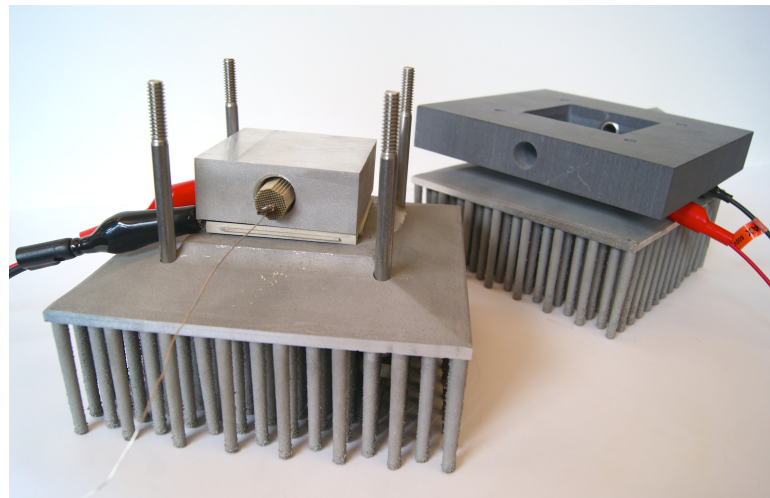
Figure 17. The initial Reactor 1 assembly is shown in two sections. During later testing, some changes to the design were made.

5.2.1.b.   *Reactor performance.* To begin analyzing Reactor 1, thermocouples were placed inside the substrate and in an array on the surface. The primary goal of these experiments was to compare combustion characteristics of

33

Reactor 1 with those of the previous cylindrical reactor, and to study temperature distribution on the surface. Figure 18 displays the substrate temperature profiles of two consecutive runs, with two cycles each. The test used a 4SSC substrate with a flow rate of 400 mL/min. The large thermal mass of Reactor 1 acted as a sink at the start of each cycle, creating a large drop in temperature after ignition. Once the reactor temperature increased, combustion temperatures rose and reached a stable plateau. The reactor mass did not cool completely to room temperature in 30 min, so all cycles succeeding the initial cycle saw less of a drop in temperature at the start. Results demonstrated that combustion characteristics of Reactor 1 were very similar to those of the cylindrical reactor, except that the large thermal mass of the new reactor caused a drop in temperature before stabilizing. Room temperature ignition, stable combustion, and repeat cycling was achieved, matching the performance of the cylindrical reactor.
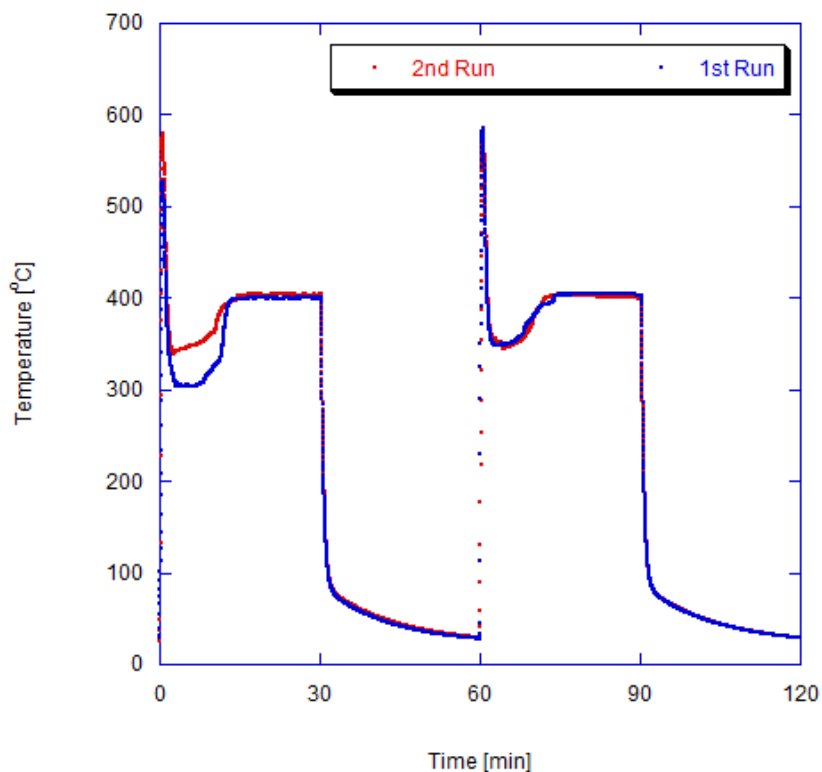
Figure 18. Substrate temperatures in Reactor 1 for 2 consecutive runs at 400 mL/min, with 2 cycles each with 4SSC substrate. The large dip in the first cycle of the first run is a result of a room temperature reactor. In the subsequent cycles the reactor was at a higher temperature at the start of combustion, and the reaction was able to reach higher temperatures more quickly.

An array of seven thermocouples was placed on the surface of the reactor to study temperature uniformity. Thermocouples were cemented and clamped between the surface of the reactor and squares of cardboard. The numbered thermocouple array can be seen in Fig. 19. As predicted through the heat transfer simulations, temperatures were extremely uniform. Figure 20 shows the surface temperature profile of each thermocouple for two cycles. The enlarged inset demonstrates that temperatures vary by less than 2 ^{o}C. The test used a 4SSC substrate with a flow rate of 400 mL/min.
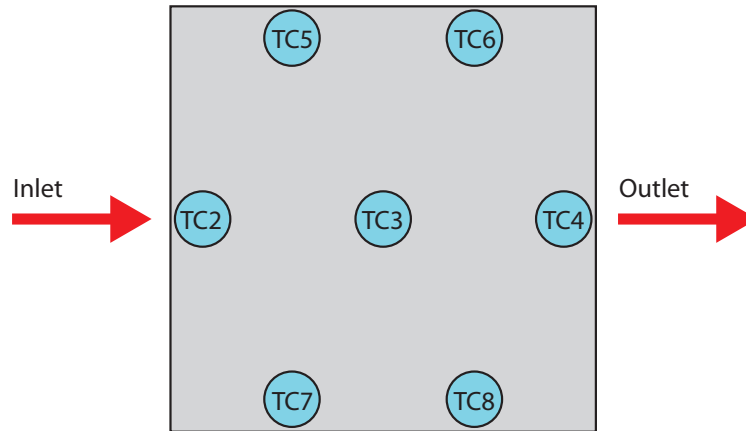
Figure 19. Seven thermocouples were placed on the top face of Reactor 1 to study temperature distribution across the surface.
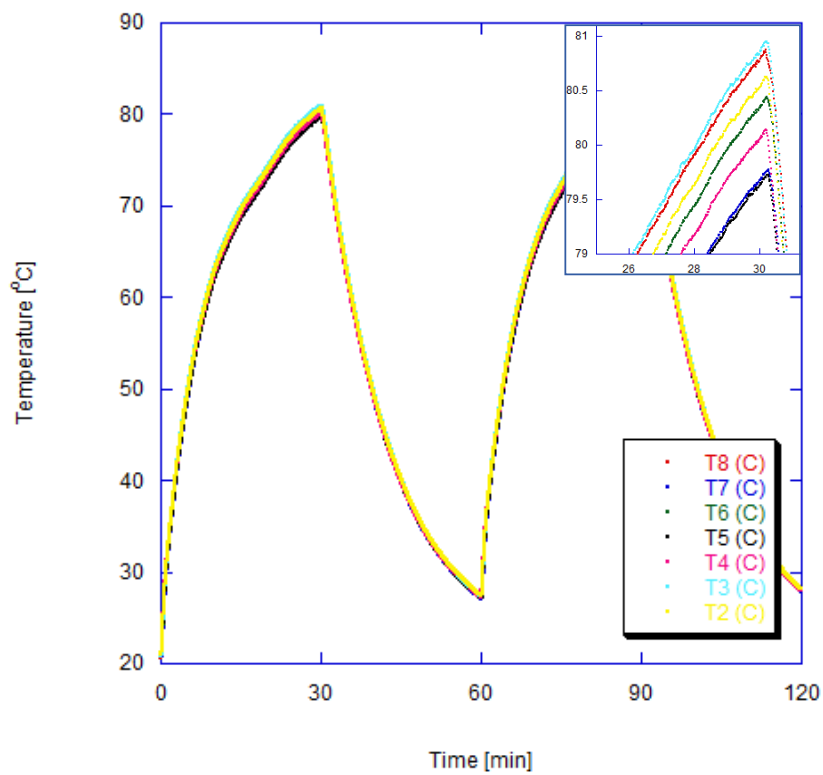
Figure 20. Surface temperatures on Reactor 1 for 1 run at 400 mL/min with 2 cycles. Temperatures are highly uniform and are still increasing at the end of a 30-minute cycle. 4SSC substrate.

After characterizing combustion and surface temperature distribution of Reactor 1, the ceramic insulation was added. The alumina silicate had been cut to fit the reactor securely inside, thereby insulating the exposed sides. As before, cardboard squares were clamped to the reactor top and bottom faces. Substrate temperatures were recorded for multiple runs to study the impact of the insulation on combustion inside the reactor. Tests used a 4SSC substrate with a flow rate of 400 mL/min. Figure 21 depicts two separate runs of two cycles each using different substrates. The gray curve represents what a normal temperature profile should look like. The extreme decrease in temperature after ignition, and subsequent failed combustion, indicates that the insulation was creating the opposite of the desired effect, and removing thermal energy from the reactor. Because the insulation was acting as a large sink, the ceramic was removed for further experiments.
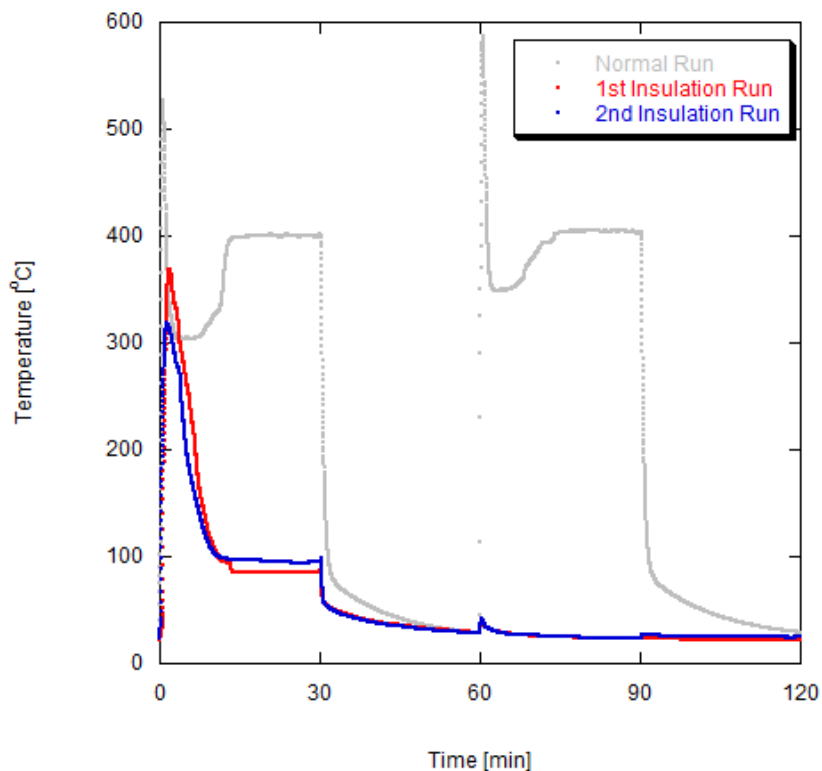
Figure 21. Substrate temperatures in Reactor 1 with ceramic insulation in place for 2 separate substrates. Each was run once at 400 mL/min for 2 cycles. The gray curve represents a normal temperature profile for the reactor without insulation. 4SSC substrate.

The device was assembled with heat sinks of varying sizes in order to choose the type that provided maximum cooling of the thermoelectric generator without affecting combustion. The device was assembled with thermoelectric modules and medium heat sinks (8 cm), large heat sinks (15 cm), or no heat sinks. At this point in testing, only one of each of the medium heat sinks was available, while there were two large sinks available. Therefore, medium heat sink tests used two different heat sinks that were expected to remove similar quantities of thermal energy. In these tests, the large heat sink refers to the rightmost sink in Fig. 10, while the medium sink refers to the second and third heat sinks from the right. Each test used a substrate with 4SSC and a flow rate of 400 mL/min. Figure 22 displays substrate temperature for each of

the three experiments. As the size of the heat sink increased, combustion stability decreased drastically. When the medium sinks were used, combustion temperature dropped significantly at first, and then regained stability after the reactor temperature increased. When the large sinks were used, combustion temperature behaved similarly to that when using the ceramic insulation. The thermal energy losses were too great to sustain combustion, and the second cycle failed to ignite fully.
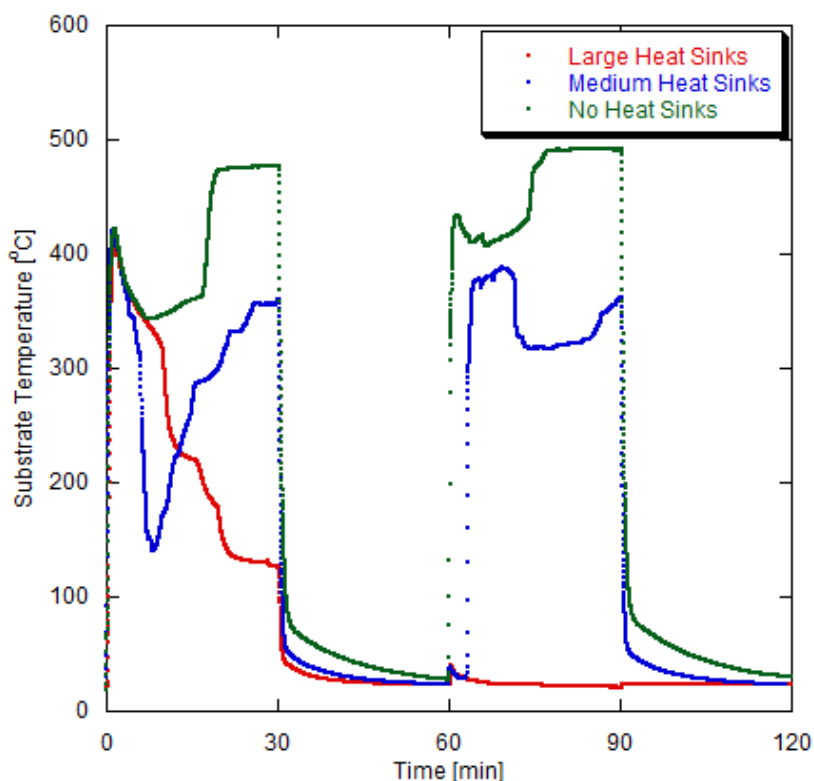
Figure 22. Substrate temperatures in Reactor 1 with full assembly using 3 sets of heat sinks with varying sizes. As the size of the heat sinks increases, combustion becomes less stable. Each was run once at 400 mL/min for 2 cycles. 4SSC substrate.

Thermocouples were placed between the thermoelectric modules and the reactor, and between the thermoelectric modules and the heat sinks, or cardboard if no heat sinks were used. These were used to study the temperature difference

across the thermoelectric modules. Larger temperature differences and higher hot side temperatures are desired to generate maximum power output. Hot- and cold-side temperatures over a single test cycle for each heat sink option can be seen in Fig. 23. Note that each color pair shows both a hot- and cold-side temperature profile. Green, blue, and red lines represent no heat sinks, medium heat sinks, and large heat sinks, respectively. With no heat sinks, the temperature difference was minimal, only 7 ^{o}C, approximately. Both the medium and large heat sinks created a temperature difference of around 13 ^{o}C. However, the thermoelectric module temperatures were slightly higher with the medium sinks and would produce more power than a system with the large heat sinks, even if stable combustion could be achieved with those heat sinks.
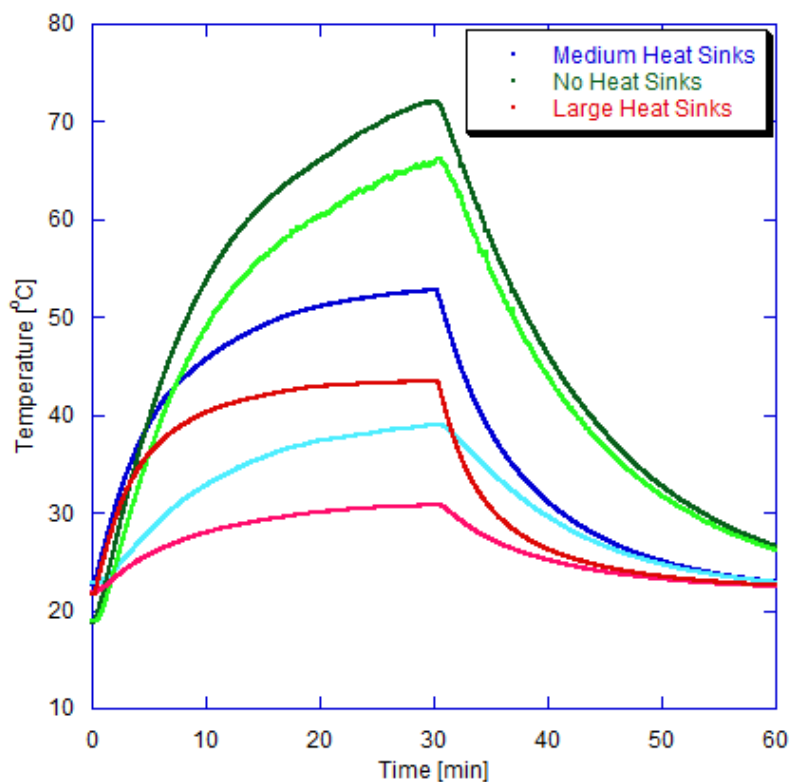
Figure 23. Thermoelectric hot- and cold-side temperatures in Reactor 1 with full assembly using 3 sets of heat sinks with varying sizes. Green, blue, and red lines represent no heat sinks, medium heat sinks, and large heat sinks, respectively. Each color pair shows both a hot-side (dark) and a cold-side (light) temperature profile. As the size of the heat sinks increases, hot-side temperature decreases. Each was run once at 400 mL/min for 2 cycles. 4SSC substrate.

Average temperature difference was taken for each heat sink option. All averages were based on the last temperature values that were recorded before the flow was turned off and temperature began to decrease. Averages were calculated by taking the mean of this temperature point for all cycles of a given test, for both the hot- and cold-side temperatures. Then difference of the average hot-side temperature and average cold-side temperature was calculated to obtain the average delta. Expected power output was calculated using a module properties spreadsheet provided by Hi-Z. Power output depends on both the hot-side temperature and the

size of the temperature difference. The temperature difference and expected power output for each heat sink option was plotted in Fig. 24. As stated earlier, the minimal temperature difference created by having no heat sinks generated very little power. The medium and large heat sinks created enough of a temperature difference to create much more power, relatively speaking. The assembly with the medium heat sinks generated the largest power output both because of a slightly larger temperature difference and higher hot-side temperature.
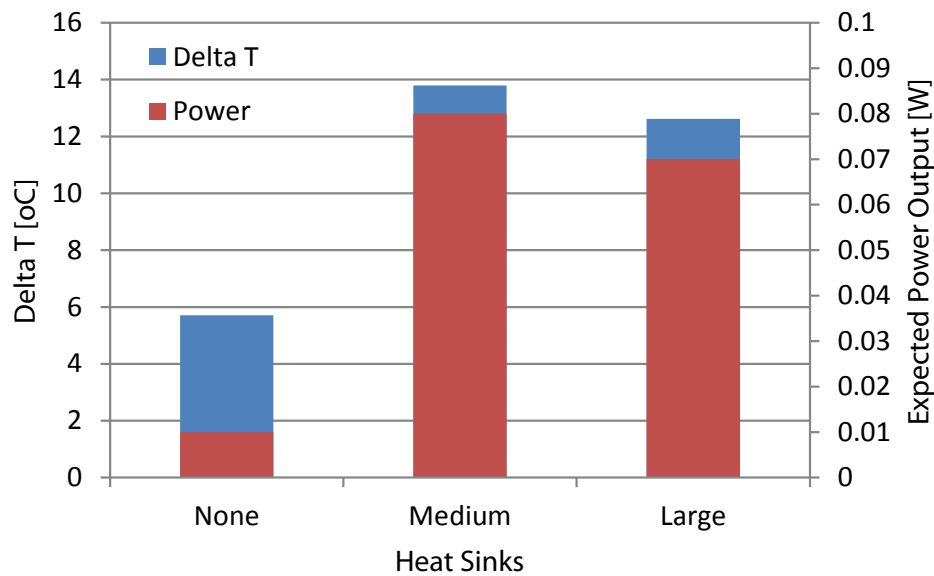
Figure 24. Average temperature difference and expected power output is shown for each heat sink option. The medium heat sinks created the largest temperature difference, while maintaining high hot-side temperatures, thereby generating the largest output.

Although tests were successful and a small power output was obtained, it was decided that the reactor needed to be redesigned. It was apparent that the large thermal mass of the current reactor was creating many issues with combustion. The more efficient heat sinks could not be used to generate larger temperature deltas over the thermoelectric generators because they were removing too much heat and causing the reaction to quench.

5.2.2. 1.2-inch planar design. This section discusses Reactor 2, the 1.2-inch planar design. The section is broken into two subsections, Development and Modeling, and Reactor Performance.

5.2.2.a. Development and modeling. A second reactor was designed with the objective of reducing thermal mass. The length and width were reduced to 1.2 inches, thereby creating hot-side surfaces with dimensions matching those of the HZ-2 thermoelectric generator. A substrate location study was conducted to determine the optimal substrate position for uniform temperatures on the hot-side of the TEG modules. Substrate placement was adjusted in several designs by altering the inlet and outlet dimensions of the flow channel. As stated earlier, a substrate is inserted through the reactor outlet until it contacts the smaller-diameter inlet channel. Shortening the inlet channel locates the substrate closer to the reactor inlet, and lengthening it locates the substrate closer to the reactor outlet.

A total of six designs were modeled in SolidWorks. The first design, Reactor 2a, consisted of a geometry similar to that of Reactor 1a, but with reduced length and width (1.2 in). Thickness remained unchanged at 1 in. Reactor 2b consisted of a modified Reactor 2a, with the introduction of concave, extruded cuts in the reactor sides parallel to the flow. This feature reduced thermal mass while maintaining 1.2-inch top and bottom surfaces. Reactor 2c consisted of a modified Reactor 2b with reduced overall thickness. Reactors 2d, 2e, and 2f further reduced thickness, and shifted the internal substrate location.

As before, a comparative heat transfer study was used to decide upon those designs to ultimately fabricate. The initial and boundary conditions used in Reactor 2 models matched those of the 2.5-inch models. A major consideration in each version of Reactor 2 was a reduction in thermal mass as compared to the previous version. Each reduction resulted in a slight increase in average hot-side temperature. After reducing

mass as much as possible, subsequent designs compared different substrate locations, similar to the comparison completed with Reactor 1. Table 2 summarizes critical design aspects and surface temperature modeling results of each reactor version.

Table 2

Summary of Reactor 2 designs considered and modeled in SolidWorks Flow Simulation.

Reactor	Concave Edges	Thickness (in)	Substrate Location	T_{Hot} Avg (^{o}C)	T_{Hot} Range (^{o}C)
2a	No	1.0	Center	195	139-207
2b	Yes	1.0	Center	207	144-220
2c	Yes	0.9	Center	209	127-227
2d	Yes	0.8	Center	214	106-246
2e	Yes	0.8	Inlet	262	201-347
2f	Yes	0.8	Outlet	181	44-235

The scope of the modeling effort did not include a study of the impact of thermal spreaders or insulating materials. These options were eliminated from consideration based on results from Reactor 1 simulations and experiments.

The three designs with the highest maximum hot-side temperature were chosen for fabrication. Reactors 2d, 2e, and 2f all incorporated concave edges and a thickness of 0.8 in. Modeling results indicated that Reactor 2e would provide the highest average and maximum hot-side temperatures. Figure 25 depicts Reactor 2d, with the substrate located at the reactor center. Figure 26 depicts Reactor 2e, with the substrate located near the reactor inlet. Figure 27 depicts Reactor 2f, with the substrate located near the reactor outlet. Surface temperature profiles were generated in SolidWorks Flow Simulation.
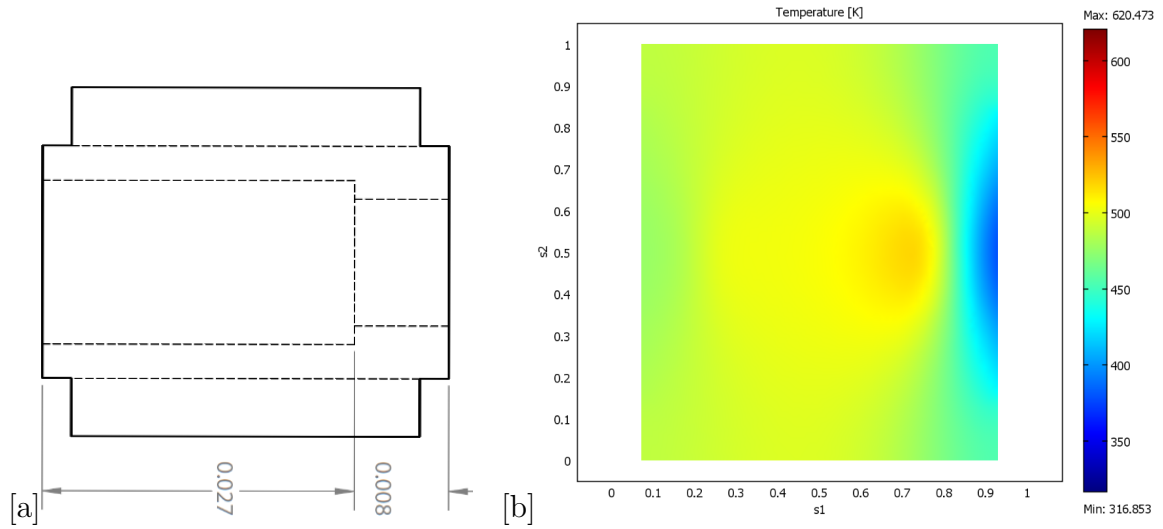
Figure 25. Reactor 2d was designed to locate the catalytic substrate at the reactor center. Subfigure (a) provides critical dimensions in meters and (b) shows surface temperature profile in Kelvin.
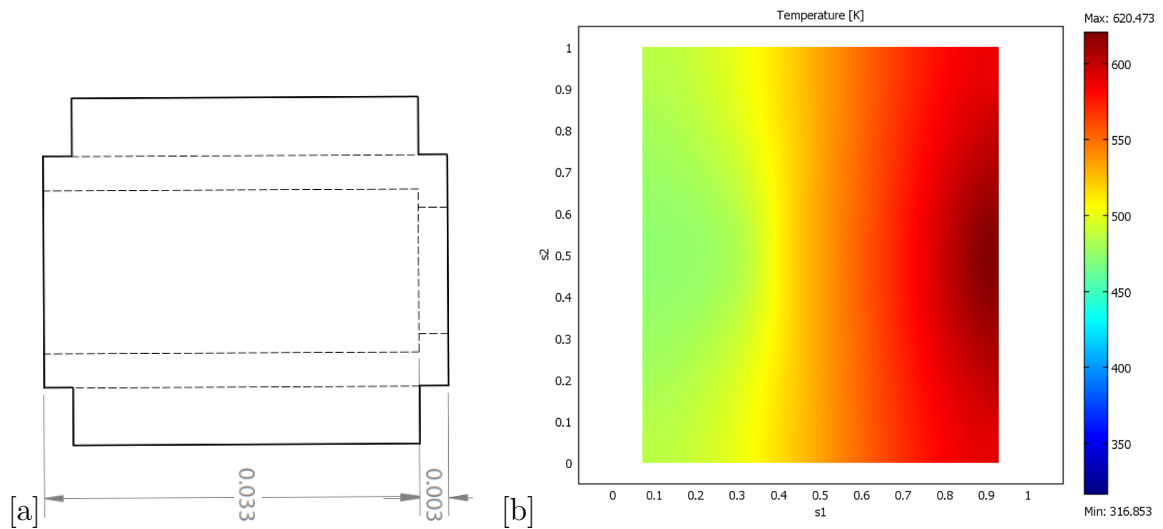
Figure 26. Reactor 2e was designed to locate the catalytic substrate near the reactor inlet. Subfigure (a) provides critical dimensions in meters and (b) shows surface temperature profile in Kelvin.
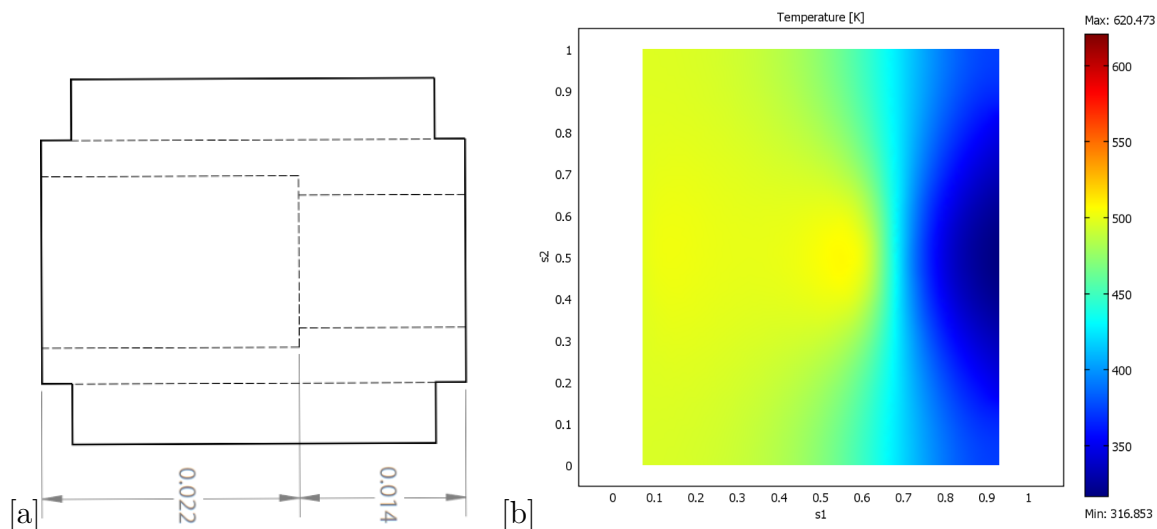
Figure 27. Reactor 2f was designed to locate the catalytic substrate near the reactor outlet. Subfigure (a) provides critical dimensions in meters and (b) shows surface temperature profile in Kelvin.

5.2.2.b. Reactor performance. To begin analysis of the second generation reactors, experiments were conducted to obtain substrate and hot-side surface temperatures for Reactors 2d, 2e, and 2f. Substrate temperature was measured in the same manner as all prior experiments. Surface temperatures were gathered from an array of five thermocouples, similar to the seven-thermocouple array used with Reactor 1 experiments. In order to simplify experiments, substrates with two sides single-coated (2SSC) were used in place of the 4SSC substrates used with Reactor 1. Substrate and hot-side surface temperatures are shown in Figure 28 for Reactors 2d, 2e, and 2f. All temperatures were collected simultaneously for each reactor experiment. Each experiment was conducted for two 30-minute cycles.
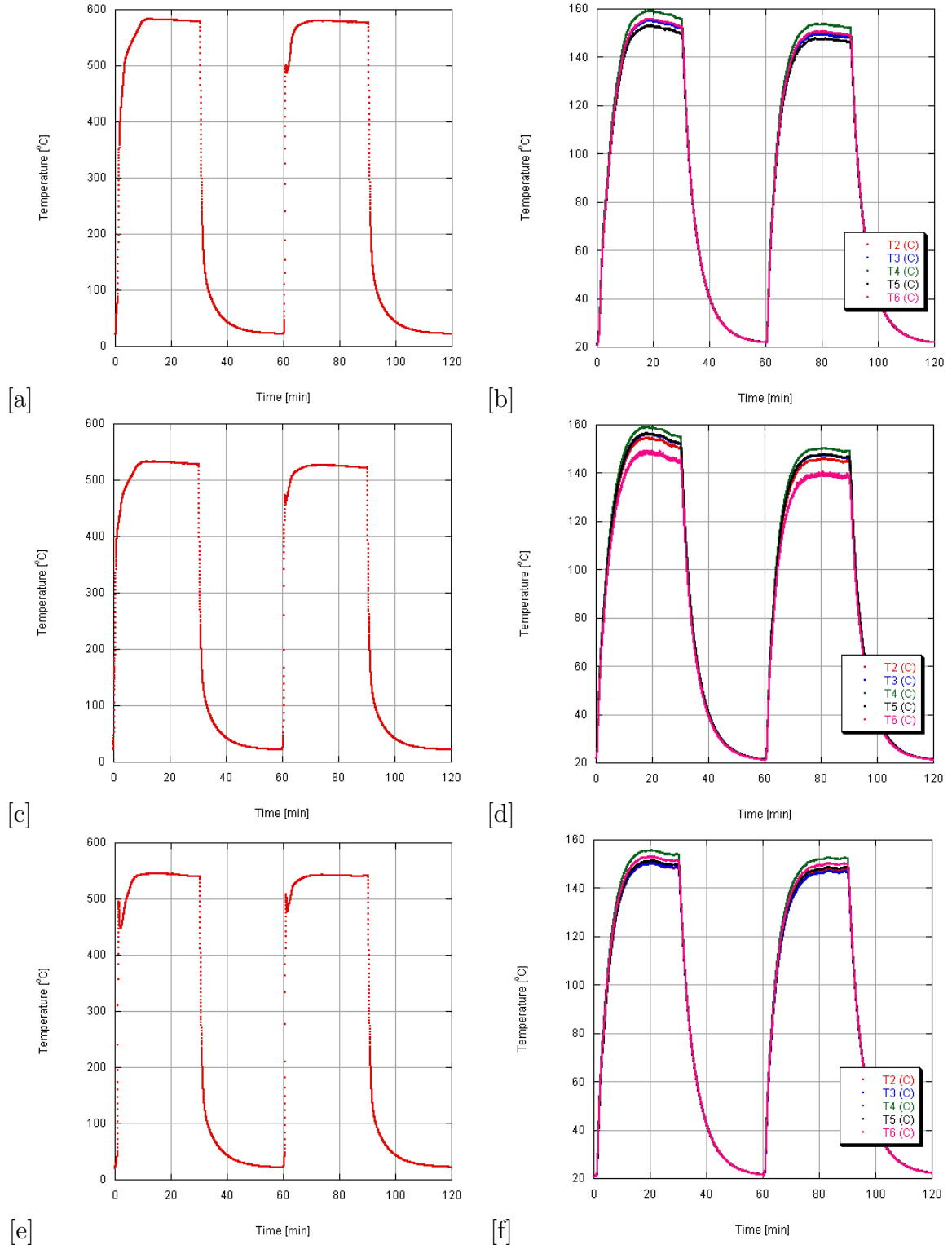
Figure 28. Temperature profiles are shown for (a) Reactor 2d substrate, (b) Reactor 2d hot-side surface, (c) Reactor 2e substrate, (d) Reactor 2e hot-side surface, (e) Reactor 2f substrate, and (f) Reactor 2f hot-side surface. Experiments were conducted using substrates with two sides single-coated (2SSC) and run for two 30-minute cycles.

These experiments upheld the comparative results of the heat transfer simulations. All reactors yielded substrate temperatures above 500 ^oC, and relatively uniform surface temperatures ranging by only 10-15 ^oC . Reactor 2e achieved surface temperatures (Subfigure 28d) similar to those of Reactor 2d (Subfigure 28b), but with a lower substrate temperature (Subfigure 28c). Reactor 2f demonstrated lower surface temperatures (Subfigure 28f) than either of the other reactors. These results demonstrated that a substrate located close to the flow inlet was ideal. The corroboration of simulation comparisons with experimental results supported a decision to eliminate Reactors 2d and 2f from consideration and continue combustion experiments with Reactor 2e only. The final Reactor 2e geometry was shown earlier in Section 4.4, Figure 9.

Further analysis of Reactor 2e performance continued with a heat sink study, similar to the Reactor 1 heat sink study. As with the 2.5-inch design, multiple heat sink pairs (with 3.5-cm, 8-cm, and 15-cm contact widths) were tested for combustion stability and impact on temperature differential across the thermoelectric modules. To begin, a baseline experiment was conducted on Reactor 2e with TEG modules but no heat sinks. Thermocouples were placed on both sides of each TEG to measure hot- and cold-side temperatures. Figure 29 shows the temperature profiles for substrate temperature and one hot- and cold-side pair of surface temperatures. With no heat sink, the temperature difference was minimal, $\sim$10-15 ^oC.
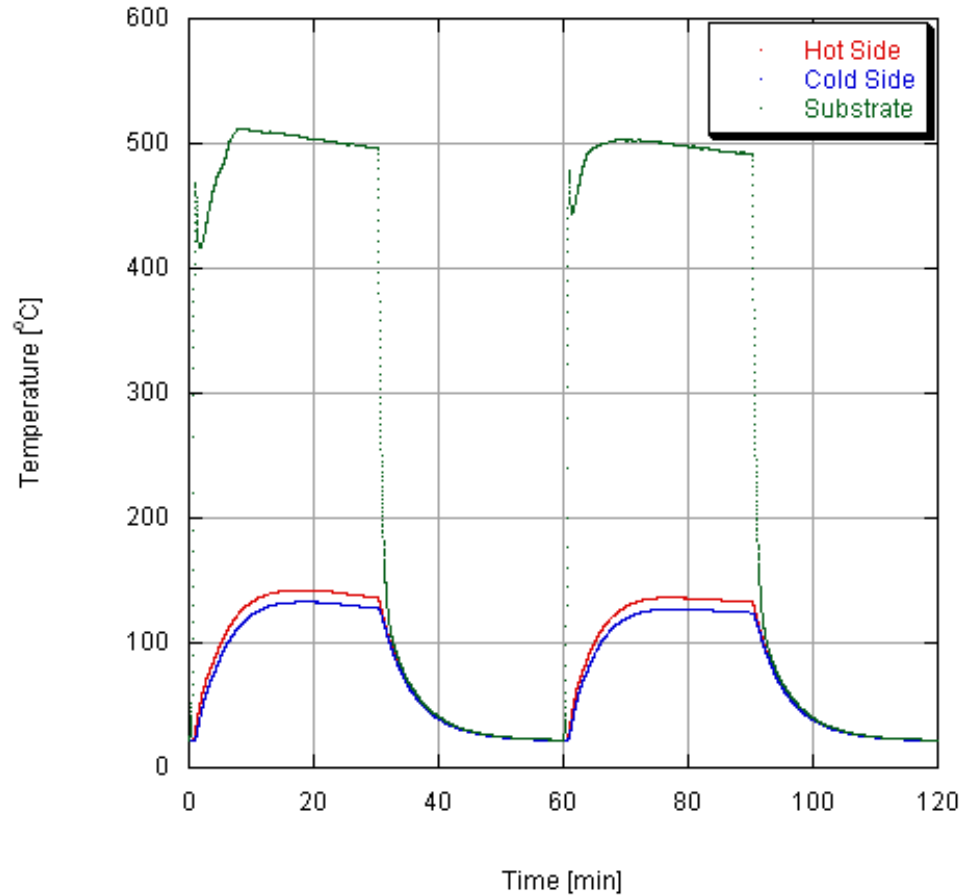
Figure 29. A baseline experiment with Reactor 2e and no heat sinks is shown. Experiment was conducted using a substrate with two sides single-coated (2SSC) and run for two 30-minute cycles.

The 3.5-cm heat sink pair was installed next, with thermocouples placed on each TEG surface. Substrate temperature and hot- and cold-side temperatures for both reactor faces are shown in Figure 30. The second plot is an enlarged view of the surface temperature profiles. Resulting temperature differentials were ~40 ^{o}C and 25 ^{o}C, for sides 1 and 2, respectively.

Figure 30. Subfigure (a) shows substrate and surface temperatures for Reactor 2e with 3.5cm heat sinks installed. Subfigure (b) shows temperature differential in more clarity in an enlarged view. Experiment was conducted using a substrate with two sides single-coated (2SSC) and run for two 30-minute cycles.

The small heat sinks were replaced with 8-cm heat sinks and further experiments were conducted. Substrate temperature and hot- and cold-side temperatures are shown in Figure 31. The second plot is an enlarged view of the surface temperature profiles. Resulting temperature differentials were ∼40 ^{o}C and 38 ^{o}C, for sides 1 and 2, respectively.

Figure 31. Subfigure (a) shows substrate and surface temperatures for Reactor 2e with 8cm heat sinks installed. Subfigure (b) shows temperature differential in more clarity in an enlarged view. Experiment was conducted using a substrate with two sides single-coated (2SSC) and run for two 30-minute cycles.

The medium heat sinks were replaced with 15-cm heat sinks and further experiments were conducted. Substrate temperature and hot- and cold-side temperatures are shown in Figure 32. The second plot is an enlarged view of the surface temperature profiles. Resulting temperature differentials were ~25 ℃ for both sides. The rapid removal of heat resulted in an unstable combustion reaction, as shown by the substrate temperature profile. Temperature dipped, and then recovered, multiple times during each 30-minute cycle. At the start of the second cycle, ignition did not fully occur for close to five minutes after the methanol-air mixture was introduced.
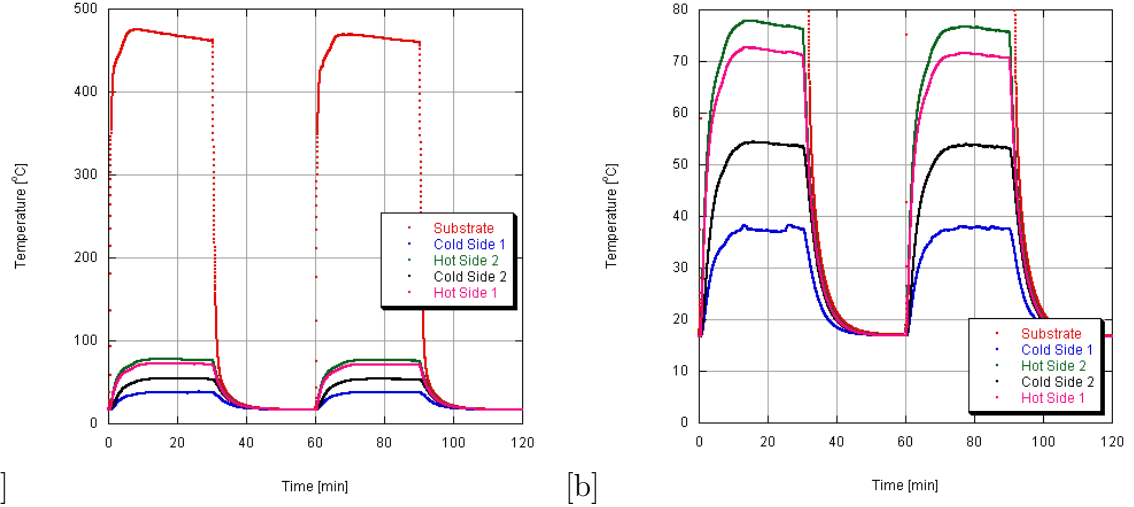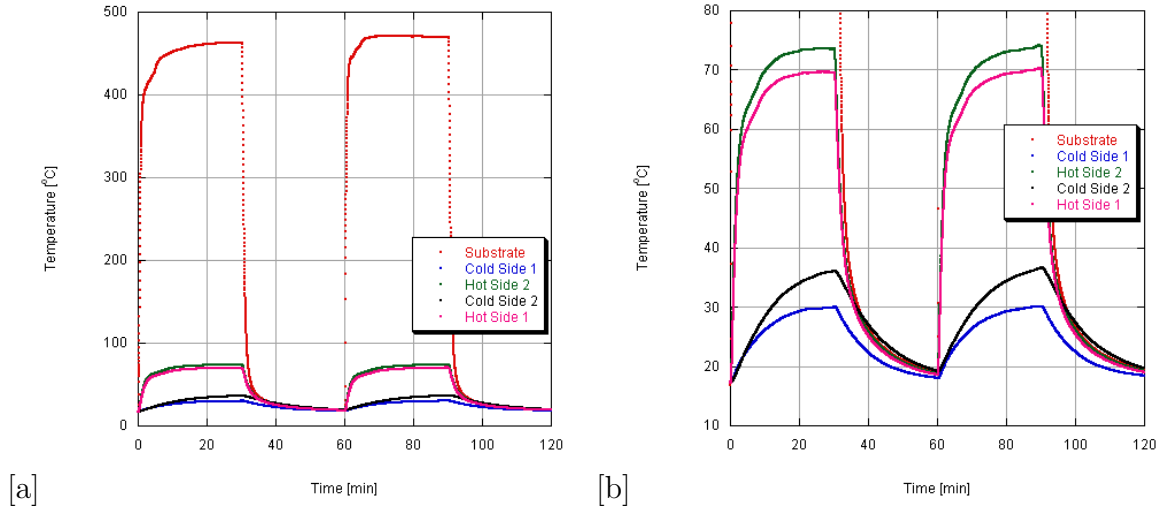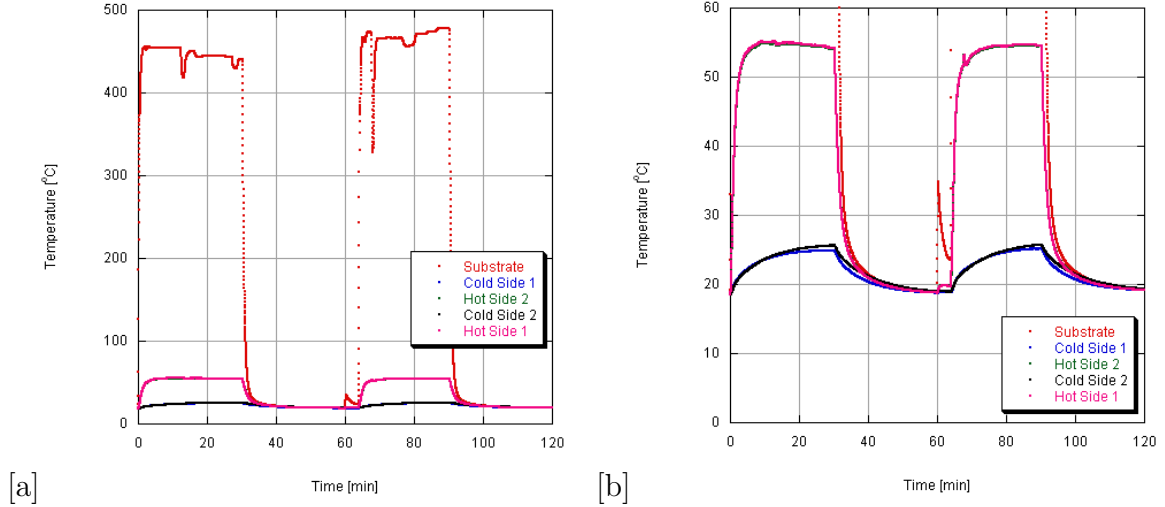
Figure 32. Subfigure (a) shows substrate and surface temperatures for Reactor 2e with 15cm heat sinks installed. Subfigure (b) shows temperature differential in more clarity in an enlarged view. Experiment was conducted using a substrate with two sides single-coated (2SSC) and run for two 30-minute cycles.

The large 15-cm heat sinks were eliminated from consideration due to combustion instability, as well as low temperature differential. The 3.5-cm heat sinks yielded a low temperature differential on one side of the reactor. As a result, the 8-cm heat sinks were selected for the MTC device.

Additional tests were conducted with a 7.6 cm-long aluminum exhaust tube attached to the reactor outlet. It was theorized that adding the exhaust tube would contain the exhaust flow and reduce heat loss to the ambient air at the reactor outlet. The exhaust tube was shown to be effective, increasing substrate temperature by ~50 °C. The exhaust tube was incorporated in the final MTC device due to these findings.

5.3. Final Design

An image of the final microcombustion-thermoelectric coupled device is shown connected to the methanol bubbler in Figure 33. The full assembly includes the 1.2-inch planar reactor (Reactor 2e) discussed in Section 5.2, medium heat sinks (8 cm), and HZ-2 TEG modules.
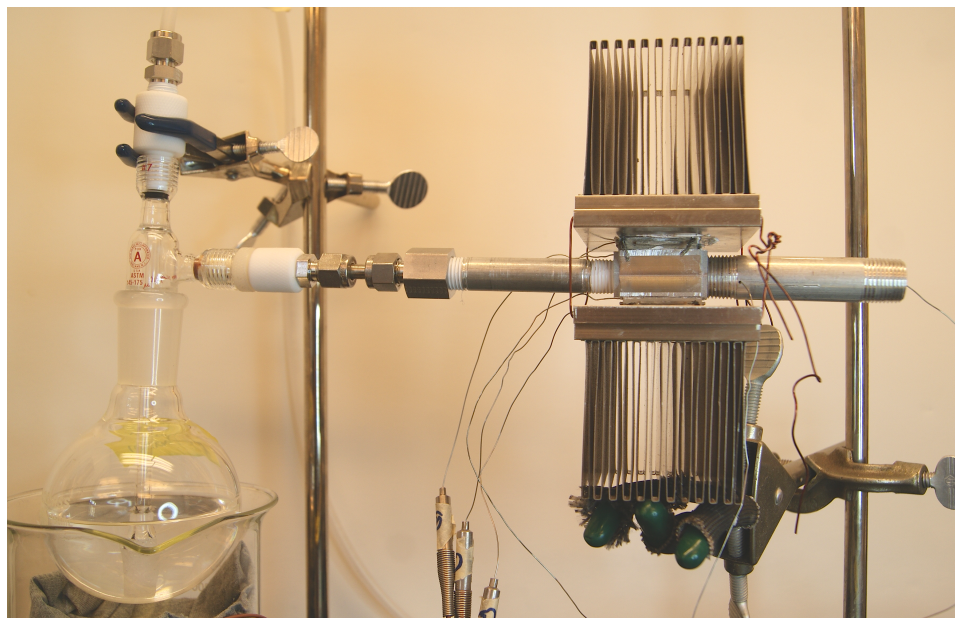
Figure 33. An image of the final MTC device assembly. Final design includes the 1.2-inch planar reactor (Reactor 2e), medium heat sinks (8 cm), and HZ-2 TEG modules.

Figure 34 presents representative temperature histories of thermocouple probes placed at key locations within the final MTC device during a typical test to assess device performance. With a flow rate of 400 mL/min, the substrate experiences the highest temperature that stabilizes within $\sim$7 min of operation. The substrate maintains the high temperature of 500 ^{o}C before returning to room temperature as the reactant mixture supply is stopped. The device symmetry is evident from the pair of hot-side and cold-side temperature profiles in Fig. 34 that directly overlap each other. The difference between the hot-side and the cold-side surface temperatures is defined as the TEG temperature difference ΔT that drives thermoelectric conversion. Considering an MTC device operates at steady conditions, ΔT at the end of a cycle is a reasonable metric to estimate device performance. Figure 34 also provides the exhaust gas temperature which is noticeably higher than the hot-side temperature and therefore indicating the future potential for harvesting the heat energy. Alternatively, the substrate temperature can be raised by increasing the flow rate through the

substrate resulting in higher heat production rate due to an increase in reactant mixture content.
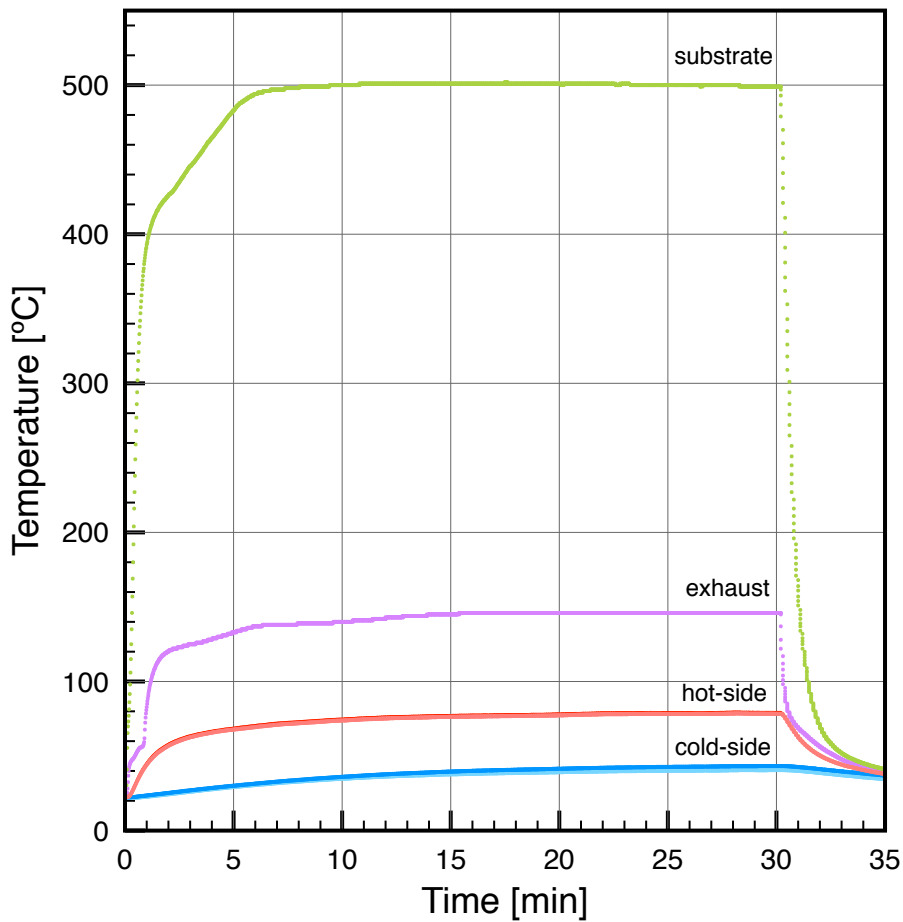
Figure 34. A single catalytic cycle for a typical run with the final MTC device showing temperature profiles for the substrate, the two hot- and cold-sides and the exhaust. Experiment conducted with flow rate 400 mL/min and 2 sides single-coated.

Figure 35 provides a summary of ΔT as a function of reactant flow rate. ΔT represent the mean temperature difference between the hot-side and the cold-side temperatures of a pair of TEGs over three consecutive catalytic cycles. The error bars represent a single standard deviation within the data subset. As Fig. 35 indicates the ΔT increases with increasing reactant flow rate up to $\sim$60 ^{o}C with 800 mL/min.

The increase in ΔT can be explained by the increased heat release as documented by our previous work [5].
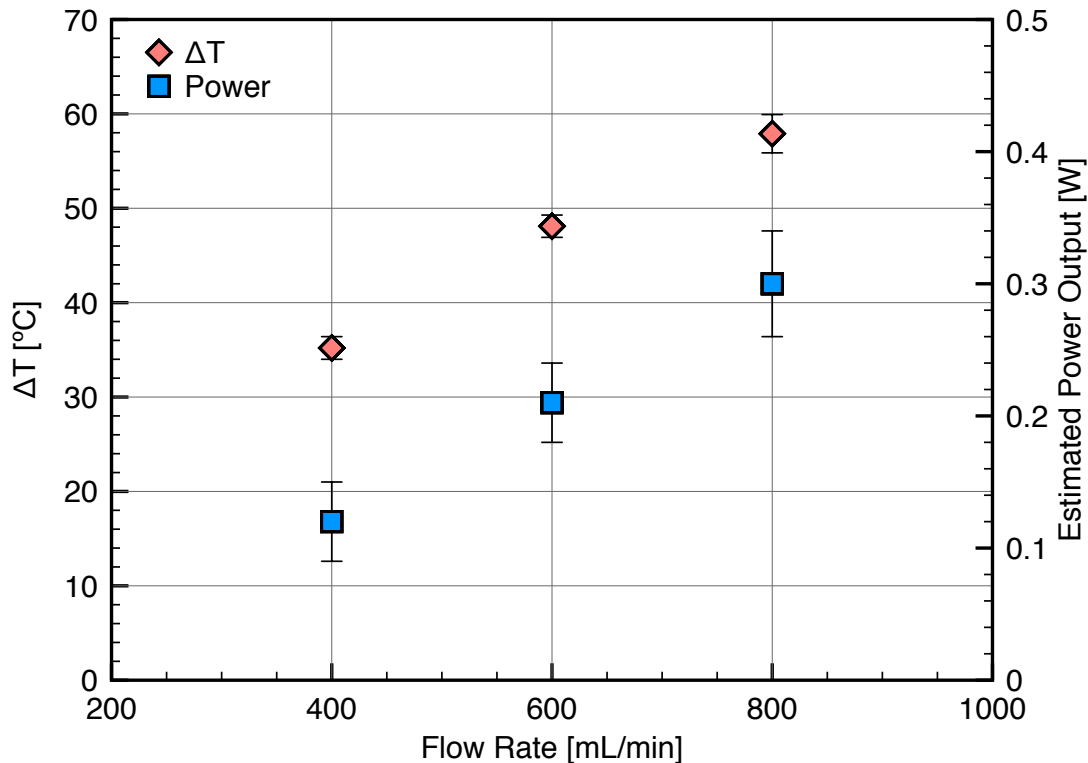
Figure 35. Average temperature difference ΔT between hot- and cold-sides of a TEG plotted as a function of flow rates. Substrate was coated on 4 sides. Error bars represent a single standard deviation. Secondary axis maps fuel-air flow rate to theoretical estimate of potential power production.

Due to system limitations, thermoelectric conversion performance was not conducted with these experiments. Instead, theoretical values for potential power output based on TEG module specifications and operational parameters (such as TEG temperature and ΔT) were obtained and plotted. Calculations used a Seebeck coefficient of 200 μV K^{-1} provided by the manufacturer. Figure 35 indicates the maximum power output at 300 mW for the highest flow rate. Assuming a nominal 60% methanol conversion rate [5], the methanol LHV and the flow rate, the energy

efficiency of the system is estimated to be 0.14%. While this value is low in comparison to hydrocarbon based power production, the state-of-the art conversion efficiencies are in the range of 2-3% [8, 4, 3, 7]. Furthermore, a number of parameters remain to be optimized within the MTC device to minimize exhaust gas temperature and maximize TEG ΔT. Several critical design parameters require further improvement, including substrate-reactor geometry, heat sink design, reactant residence time, and management of heat loss from the reactor, to name a few.

Chapter 6

Conclusion

This work provided important experimental results on design of a microcombustion-thermoelectric coupled (MTC) device using Pt nanoparticles as the catalyst. Through the evolution of reactor design, the researchers learned important lessons relating to thermal management of the combustion reaction. It was found that more thermal mass, including that of an insulating material, had a detrimental impact on combustion ignition and sustainability. Size selection of the heat sinks used to decrease TEG cold-side temperature was found to be equally important in balancing thermoelectric conversion with combustion stability. The final reactor design ultimately provided a functional device with the ability to achieve repeatable catalytic cycles using the same Pt-nanoparticle catalyst used in earlier studies at Rowan University. Tests with this reactor demonstrated room-temperature ignition and self-sustaining combustion. Surface and exhaust temperature profiles show that this reactor has significant potential, with some redesign. The substrate configuration was an aspect that was not explored as part of this thesis but it is likely the next step to optimize heat release and create a more distributed heat generation zone. Concurrent studies of fuel choices were also conducted and published along with these efforts that will help future efforts. While the efficiency of the new reactor is low, this work indicated multiple aspects of the design that can be modified to enhance performance. More importantly, the results provide a viable template towards a highly miniaturized design for a microcombustion-thermoelectric coupled power device.

Chapter 7

Follow-Up Studies

At the time of this writing, significant time has passed since the completion of the documented work. As such, in lieu of a section discussing next steps, the recent follow-on studies at Rowan University will be discussed.

Recent work at Rowan has sought to improve thermal design aspects of a nanocatalytic microcombustion-thermoelectric coupled (MTC) device. Initial improvements used the same reactor designed in this work, and focused on increased thermal contact through a redesign of the test stand. Subsequent work involved multiple redesigns of the reactor. Each redesign sought to improve thermal power generation and management, while maintaining use of a catalyst derived from that used by Appplegate et al. [5] and also in this work.

Ultimately, a fully redesigned MTC device was tested and results were published in 2019 [13]. To increase heat generation potential, the reactor was redesigned to host a larger section of catalytic substrate, prepared in a similar manner to the catalyst first used by Applegate et al. [5]. In addition to a larger combustion chamber, the new reactor incorporates two fuel inlet channels running on either side of the substrate. Reactant flow enters on the same side of the reactor as the exhaust outlet, and runs the length of the reactor before redirecting 180° into the substrate. The new design permits all inlet and outlet ports to be located on one side of the reactor, as well as permitting preheating of the reactants. The top and bottom surfaces of the reactor are comprised of copper plates to provide high thermal conductivity but low thermal mass. The microcombustor was designed to integrate with new TEG modules and heat sinks.

Tests were conducted using the same methanol-air mixture but with much higher air flow rates, 4000 - 10000 mL/min. Substrate and surface temperatures

were higher than the previous work, but resulted in a similar thermoelectric module temperature differential (ΔT ~62 ^{o}C). The combination of similar ΔT with a larger MTC configuration resulted in a theoretical power output of 1400 mW, a significant improvement on the device documented here. While measured output was only 490 mW, losses were attributed to thermal contact between the microcombustor and TEG modules.

In addition to the thermal improvements summarized above, the test facility was redesigned to take up a smaller footprint. This was done through the creation of a single structural base that supports most major components and improves portability of the test stand. The testing manifold was also designed to provide better mechanical pressure and reduce contact resistance between discrete parts of the MTC.

References

[1] A. C. Fernandez-Pello, "Micropower generation using combustion: Issues and approaches," *Proceedings of the Combustion Institute*, vol. 29, no. no. 1, pp. 883–899, 2002.

[2] L. Sitzki, K. Borer, E. Schuster, P. D. Ronney, and S. Wussow, "Combustion in Microscale Heat-Recirculating Burners," in *The Third Asia-Pacific Conference on Combustion*, 2001, pp. 1–4.

[3] J. A. Federici, D. G. Norton, T. Bruggemann, K. W. Voit, E. D. Wetzel, and D. G. Vlachos, "Catalytic microcombustors with integrated thermoelectric elements for portable power production," *Journal of Power Sources*, vol. 161, no. no. 1, pp. 1469–1478, 2006.

[4] A. M. Karim, J. A. Federici, and D. G. Vlachos, "Portable power production from methanol in an integrated thermoeletric/microreactor system," *Journal of Power Sources*, vol. 179, no. no. 1, pp. 113–120, 2008.

[5] J. R. Applegate, H. Pearlman, and S. D. Bakrania, "Catalysis of methanol-air mixture using platinum nanoparticles for microscale combustion," *Journal of Nanomaterials*, vol. 2012, no. no. 1, 2012.

[6] J. Vican, B. F. Gajdeczko, F. L. Dryer, D. L. Milius, I. A. Aksay, and R. A. Yetter, "Development of a Microreactor as a Thermal Source for Microelectromechanical Systems Power Generation," *Proceedings of the Combustion Institute*, vol. 29, pp. 909–916, 2002.

[7] K. Yoshida, S. Tanaka, S. Tomonari, D. Satoh, and M. Esashi, "High-energy density miniature thermoelectric generator using catalytic combustion," *Journal of Microelectromechanical Systems*, vol. 15, no. 1, pp. 195–203, 2006.

[8] C. H. Marton, G. S. Haldeman, and K. F. Jensen, "Portable Thermoelectric Power Generator Based on a Microfabricated Silicon Combustor with Low Resistance to Flow," *Industrial & Engineering Chemistry Research*, vol. 50, no. 14, pp. 8468–8475, jul 2011. [Online]. Available: http://pubs.acs.org/doi/abs/10.1021/ie200210d

[9] N. S. Kaisare and D. G. Vlachos, "A review on microcombustion: Fundamentals, devices and applications," *Progress in Energy and Combustion Science*, vol. 38, no. 3, pp. 321–359, jun 2012. [Online]. Available: http://linkinghub.elsevier.com/retrieve/pii/S0360128512000020

[10] F. J. Disalvo, "Thermoelectric Cooling and Power Generation," *Science*, vol. 285, no. 5428, pp. 703–706, 1999.

[11] S. Leblanc, S. K. Yee, M. L. Scullin, C. Dames, and K. E. Goodson, "Material and manufacturing cost considerations for thermoelectrics," *Renewable and Sustainable Energy Reviews*, vol. 32, pp. 313–327, 2014. [Online]. Available: http://dx.doi.org/10.1016/j.rser.2013.12.030

[12] F. Bonet, V. Delmas, S. Grugeon, R. H. Urbina, and P.-y. Silvert, "Synthesis of Monodisperse Au, Pt, Pd, Ru and Ir Nanoparticles in Ethylene Glycol," *NanoStructured Materials*, vol. 11, no. 8, pp. 1277–1284, 1999.

[13] B. R. Guggilla, A. Rusted, and S. Bakrania, "Platinum nanoparticle catalysis of methanol for thermoelectric power generation," *Applied Energy*, vol. 237, no. January, pp. 155–162, 2019. [Online]. Available: https://doi.org/10.1016/j.apenergy.2018.12.083

[14] Z. Hu, V. Boiadjiev, and T. Thundat, "Nanocatalytic Spontaneous Ignition and Self-Supporting Room-Temperature Combustion," *Energy & Fuels*, vol. 19, no. 4, pp. 855–858, 2005.

[15] E. L. Dreizin, "Metal-based reactive nanomaterials," *Progress in Energy and Combustion Science*, vol. 35, no. 2, pp. 141–167, apr 2009. [Online]. Available: http://linkinghub.elsevier.com/retrieve/pii/S0360128508000646

[16] D. G. Norton, K. W. Voit, T. Brüggemann, and D. G. Vlachos, "Portable power generation via integrated catalytic microcombustion-thermoelectric devices," University of Delaware, Dept. of Chemical Engineering and Center for Composite Materials, Newark, DE, Tech. Rep., 2004.

[17] J. Ahn, C. Eastwood, L. Sitzki, and P. D. Ronney, "Gas-phase and catalytic combustion in heat-recirculating burners," *Proceedings of the Combustion Institute*, vol. 30, no. 2, pp. 2463–2472, 2005. [Online]. Available: http://dx.doi.org/10.1016/j.proci.2004.08.265